Supplementary Information

for

Core-Wing Modulated Squaraines with Enhanced Two-Photon Absorption and Efficient Photothermal Eradication of Bacteria

Xin-Ao Liu,[1] Xingtong Zhou,[1] Tong Zhang,[2] Congdi Shang,*[,2] Liping Ding,*[,1] Taihong Liu,*[,1] and Yu Fang[1]

[1] *Key Laboratory of Applied Surface and Colloid Chemistry of Ministry of Education, Shaanxi Provincial Key Laboratory of New Concept Sensors and Molecular Materials, School of Chemistry and Chemical Engineering, Shaanxi Normal University, Xi'an 710119, P. R. China*

[2] *College of Food Science and Engineering, Northwest A&F University, Shaanxi, Yangling 712100, P. R. China*

Corresponding authors: liuth121@snnu.edu.cn (T. Liu); dinglp33@snnu.edu.cn (L. Ding); shangcd@nwafu.edu.cn (C. Shang)

Contents

1. Experimental section

1.1. Materials and methods

All the reagents and solvents were commercially available without further purification unless otherwise noted. Thin-layer chromatography (TLC) was performed on the precoated silica gel 60 F254 plates and column chromatography was performed over silica gel 230 ~ 400 mesh. NMR (^{1}H and ^{13}C) measurements were performed at room temperature by a Bruker Avance III NMR spectrometer with tetramethylsilane (TMS) as an internal reference. High-resolution mass spectra (HRMS) were acquired in Electrospray Ionization (ESI) sources using a Bruker maXis UHR-TOF mass spectrometer. The optical properties of the dyes were investigated in the spectroscopic-grade solvents. Ultrapure water (resistivity >18.0 MΩ·cm) was obtained from a Millipore Milli-Q system. UV-vis spectra were recorded using Shimadzu UV-2600 spectrometer and Perkin Elmer Lambda 1050 spectrometer in 10.0 mm path quartz cuvettes. The corresponding full width at half maximum (FWHM) was calculated properly. Steady-state fluorescence emission spectra were obtained using a fluorescence spectrometer (Edinburgh FLS1000) with a xenon lamp as the light source at room temperature. Fluorescence lifetimes (τ_F) were determined by the time-correlated single photon counting technique (TCSPC) with the same Edinburgh spectrometer using a pulsed picosecond diode laser (EPL-405) as the excitation source. The instrument response function (IRF) was measured by monitoring a scattering solution of colloidal silica (Ludox). It should be mentioned that the maximum optical density of the investigated solutions did not exceed 0.1 and all reabsorption effects were negligible. The absolute fluorescence quantum yields (Φ_F) were obtained using a Hamamatsu C9920-02G instrument with a Xe excitation source and a Hamamatsu A10080-01 monochromator. Details of plant fluorescence imaging could be found in the reported literatures by our group. [1] *Escherichia coli* (ATCC 25922) was acquired from the Lab of Food Microbiology and Food Biotechnology in Northwest A&F University (Yangling, Shaanxi).

1.2. Antibacterial capacity determination

Standard strain of *Escherichia coli* (ATCC 25922) was selected as the target bacteria. The bacteria were cultured in a liquid medium at 37 °C for 12 h to reach a concentration of 10^8 CFU/mL. Antibacterial experiments were conducted by mixing the diluted bacterial suspension and the investigated squaraines (SQs) solution, the blank group without SQs was treated identically. The mixtures were then exposed simultaneously to a xenon lamp (50 mW/cm²) and an 808 nm NIR laser (2.0 W/cm^2). After irradiation, 100 μL of each sample from both the control and experimental groups was

evenly spread on LB agar plates and incubated at 37 °C for 12 h. Photographs were taken to observe bacterial colony growth and evaluate bactericidal efficacy.

$$\text{Survival rate (\%)} = \frac{bacterialog\ (CFU/mL)\ after\ irradiation}{bacterialog\ (CFU/mL)\ of\ blank\ group}$$

The data were represented as the mean ± standard deviation (SD), and all the experiments were triplicated.[2]

1.3. Calculation details of the optical bandgaps

Transition dipole moments ($\Delta\mu$) between the ground state (S_0) and the excited states were obtained by integration of the main low energy absorption bands of the squaraines (SQs) and calculated as follows:

$$\Delta\mu = 0.09584 \times \sqrt{\int \frac{\varepsilon(\nu)}{\nu^{max}} d\nu}$$

Where $\varepsilon(\nu)$ is the molar extinction coefficient of transition, ν^{max} is the maximum absorption wavelength in cm^{-1}.[3] The transition dipole moment $\Delta\mu_{01}$ was denoted for the transition from S_0 to the first excited state (S_1).

The optical bandgap (E_g^{opt}) is obtained according to the following equation, E_g^{opt} (eV) = 1240/λ_{edg}, where λ_{edg} is the onset value of absorption spectrum in the long wavelength direction.[3]

2. Synthesis and characterization

2.1. General procedures for synthesizing the SQs

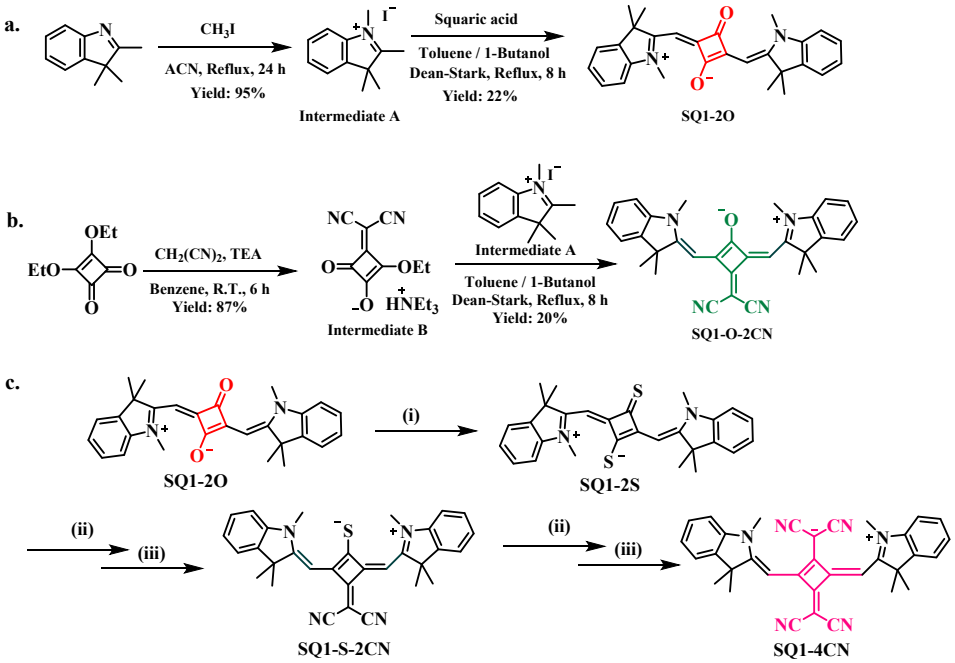

Reaction Conditions: (i) Lawesson Reagent, Toluene, N_2, 100°C, 2 h; (ii) $CF_3SO_3CH_3$, DCM, N_2, R.T., 0.5 h; (iii) $CH_2(CN)_2$, EtOH, TEA, N_2, Reflux.

Scheme S1 Synthesis routes for the dyes SQ1-2O (a), SQ1-O-2CN (b), and SQ1-4CN (c).

The symmetrical SQs were generally prepared by reacting squaric acid (1,2-dihydroxy-1-cyclobutene-3,4-dione) with two equivalents of the electron-donating heterocycle in refluxing 1-butanol/toluene with an apparatus of Dean-Stark, where the generated water was removed continuously. The dyes SQ1-2O, SQ1-O-2CN, and SQ1-4CN were synthesized according to the versatile and straightforward methods (Scheme S1).[4,5] To be noted, the intermediate 1,2,3,3-tetramethyl-3*H*-indolium indolenine (the intermediate A) and triethylammonium-3-(dicyanomethylene)-2-ethoxy-4-oxocyclobut-1-enolate (the intermediate B) were synthesized in the literatures with high yields of 95% and 87%, respectively.[6,7]

2.2. Synthesis and characterization of the dye SQ2-2O

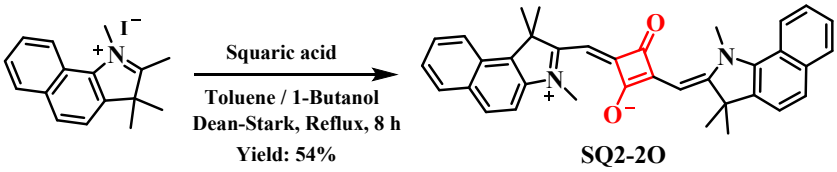

Scheme S2 Synthesis route for the dye SQ2-2O.

A mixture of 1,2,3,3-tetramethyl-1*H*-benzo[e]indol-3-ium iodide (1.40 g, 4.0 mmol) and squaric acid (0.23 g, 2.0 mmol) in 1-butanol/toluene (1/1, *v*/*v*, 100 mL) was refluxed for 8 h with a Dean-Stark apparatus. After cooling down to room temperature, solid precipitate was collected by filtration. Further purification was carried out by column chromatography using dichloromethane/methanol (150/1, *v*/*v*) as the eluent to yield the green dye SQ2-2O (0.57 g, yield 54%). ^{1}H NMR ($CDCl_3$, 600 MHz, ppm): δ 8.20 (d, J = 8.6 Hz, 2H, Ar-*H*), 7.89 (dd, J = 11.4, 8.4 Hz, 4H, Ar-*H*), 7.60-7.56 (m, 2H, Ar-*H*), 7.42 (s, 2H, Ar-*H*), 7.33 (s, 2H, Ar-*H*), 6.02 (s, 2H, C=C-*H*), 3.70 (s, 6H, -NCH_3), 2.07 (s, 12H, -C(CH_3)$_2$). ^{13}C NMR ($CDCl_3$, 151 MHz, ppm): δ 131.42, 129.78, 128.63, 127.41, 124.45, 122.57, 110.01, 53.41, 51.20, 26.73. HRMS (ESI, [M+Na]$^+$, *m*/*z*): calculated for $C_{36}H_{32}N_2O_2Na^+$: 547.2356, found: 547.2357.

2.3. Synthesis and characterization of the dye SQ2-O-2CN

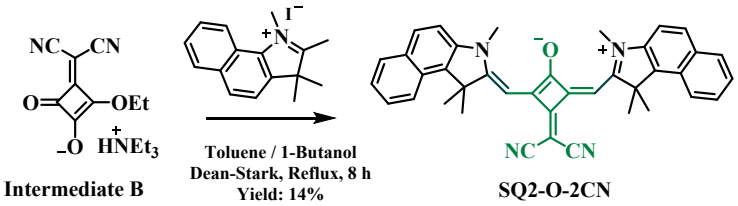

Scheme S3 Synthesis route for the dye SQ2-O-2CN.

A mixture of intermediate B (triethylammonium-3-(dicyanomethylene)-2-ethoxy-4-oxocyclobut-1-enolate, 0.20 g, 1.0 mmol) and 1,2,3,3-tetramethyl-1*H*-benzo[e]indol-3-ium iodide (0.72 g, 2.1 mmol) in 1-butanol/toluene (1/1, *v*/*v*, 40

mL) was refluxed for 8 h with a Dean-Stark apparatus. After cooling down to room temperature, solid precipitate was collected by filtration. Further purification was carried out by column chromatography using dichloromethane/methanol (100/1, *v*/*v*) as the eluent to yield the dark red dye SQ2-O-2CN (0.83 g, yield 14%). ^{1}H NMR ($CDCl_3$, 600 MHz, ppm): δ 8.18 (d, J = 8.5 Hz, 2H, Ar-*H*), 7.93 (t, J = 8.4 Hz, 4H, Ar-*H*), 7.60 (t, J = 7.6 Hz, 2H, Ar-*H*), 7.46 (s, 2H, Ar-*H*), 7.37 (d, J = 8.7 Hz, 2H, Ar-*H*), 6.53 (s, 2H, C=C-*H*), 3.77 (s, 6H, -NCH_3), 2.05 (s, 12H, -C(CH_3)$_2$). HRMS (ESI, [M+Na]$^+$, *m*/*z*): calculated for $C_{39}H_{32}N_4ONa^+$: 595.2468, found: 595.2479.

2.4. Synthesis and characterization of the dye SQ2-4CN

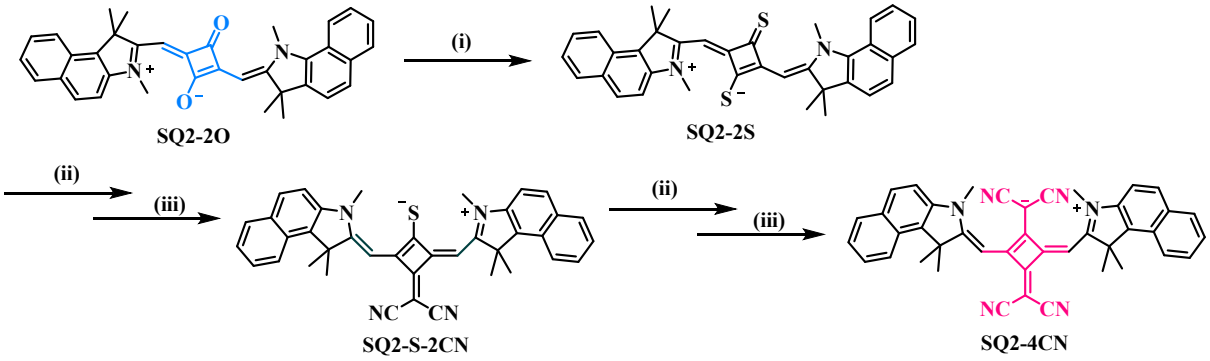

Reaction Conditions: (i) Lawesson Reagent, Toluene, N_2, 100°C, 2 h; (ii) $CF_3SO_3CH_3$, DCM, N_2, R.T., 0.5~1.5 h; (ii) $CH_2(CN)_2$, EtOH, TEA, N_2, Reflux.

Scheme S4 Synthesis route for the dye SQ2-4CN.

As shown in Scheme S4, a mixture of SQ2-2O (0.46 g, 0.9 mmol) and Lawesson reagent (0.71 g, 1.8 mmol) in 60 mL dry toluene was refluxed for 2 h under nitrogen atmosphere. After cooling down to room temperature, solid precipitate was collected by filtration and purification was carried out by column chromatography using dichloromethane/methanol (200/1, *v*/*v*) as the eluent to yield the golden dye SQ2-2S (0.54 g, yield 59%). ^{1}H NMR ($CDCl_3$, 600 MHz, ppm): δ 8.17 (d, J = 8.5 Hz, 2H, Ar-*H*), 7.93 (dd, J = 8.5, 4.7 Hz, 4H, Ar-*H*), 7.59 (t, J = 7.7 Hz, 2H, Ar-*H*), 7.46 (t, J = 7.5 Hz, 2H, Ar-*H*), 7.38 (d, J = 8.7 Hz, 2H, Ar-*H*), 6.32 (s, 2H, C=C-*H*), 3.95 (s, 6H, -NCH_3), 2.04 (s, 12H, -C(CH_3)$_2$). ^{13}C NMR ($CDCl_3$, 151 MHz, ppm): δ 186.16, 166.13, 140.54, 134.12, 131.65, 129.88, 129.79, 128.59, 127.45, 124.74, 122.65, 110.59, 86.68, 51.82, 27.35. HRMS (ESI, [M+H]$^+$, *m*/*z*): calculated for $C_{36}H_{33}N_2S_2^+$: 557.2080, found: 557.2078.

A mixture of SQ2-2S (0.71 g, 1.3 mmol) and methyl trifluoromethanesulfonate (0.63 g, 3.8 mmol) in 60 mL dry chloroform was heated for 2 h under nitrogen atmosphere. After cooling down to room temperature, the solvent was evaporated under reduced pressure, and a dark blue solid intermediate was obtained. Then, a mixture of crude intermediate, malononitrile (0.17 g, 2.6 mmol), and catalytic amount of triethylamine in dry ethanol (60 mL) was heated

for 1.0 h under nitrogen atmosphere. After ending the reaction, the solvent was removed by rotational evaporation and the residue was purified by column chromatography (150/1, *v*/*v*, dichloromethane/methanol on silica) to yield SQ2 -S-2CN as a black solid (0.14 g, yield 18%). ^{1}H NMR ($CDCl_3$, 600 MHz, ppm): δ 8.09 (d, J = 8.5 Hz, 2H, Ar-*H*), 7.94 (dd, J = 8.7, 2.7 Hz, 4H, Ar-*H*), 7.60 (t, J = 7.6 Hz, 2H, Ar-*H*), 7.48 (d, J = 8.0 Hz, 2H, Ar-*H*), 7.39 (d, J = 8.7 Hz, 2H, Ar-*H*), 6.11 (s, 2H, C=C-*H*), 3.96 (s, 6H, -NCH_3), 1.88 (s, 12H, -C(CH_3)$_2$). HRMS (ESI, [M+Na]$^+$, *m*/*z*): calculated for $C_{39}H_{32}N_4SNa^+$: 611.2240, found: 611.2250.

A mixture of SQ2-S-2CN (0.39 g, 0.7 mmol) and methyl trifluoromethanesulfonate (0.48 g, 3.00 mmol) in 40 mL dry chloroform was heated for 2 h under nitrogen atmosphere. After cooling down to room temperature, the solvent was evaporated under reduced pressure and a dark blue solid intermediate was obtained. Then, a mixture of crude intermediate, malononitrile (0.09 g, 1.3 mmol), and catalytic amount of triethylamine in dry ethanol (50 mL) was heated for 2 h under nitrogen. After ending the reaction, the solvent was removed by rotational evaporation. The residue was purified by column chromatography (200/1, *v*/*v*, dichloromethane/methanol on silica) to yield the dye SQ2-4CN as a black solid (0.03 g, yield 9%). ^{1}H NMR (DMF-d_7, 600 MHz, ppm): δ 8.33 (d, J = 8.5 Hz, 2H, Ar-*H*), 8.18 (d, J = 8.8 Hz, 2H, Ar-*H*), 8.15-8.11 (m, 2H, Ar-*H*), 7.81 (d, J = 8.8 Hz, 2H, Ar-*H*), 7.70 (s, 2H, Ar-*H*), 7.58 (d, J = 8.1 Hz, 2H, Ar-*H*), 6.05 (s, 2H, C=C-*H*), 4.21 (s, 6H, -NCH_3), 1.84 (s, 12H, -C(CH_3)$_2$). ^{13}C NMR (DMF-d_7, 151 MHz, ppm): δ 204.4, 178.3, 162.7, 162.5, 157.7, 152.6, 142.6, 133.7, 131.0, 129.0, 128.4, 125.9, 117.8, 112.7, 84.68, 52.8, 45.6, 25.62. HRMS (ESI, [M+Na]$^+$, *m*/*z*): calculated for $C_{34}H_{28}N_6Na^+$: 643.2581, found: 643.2588.

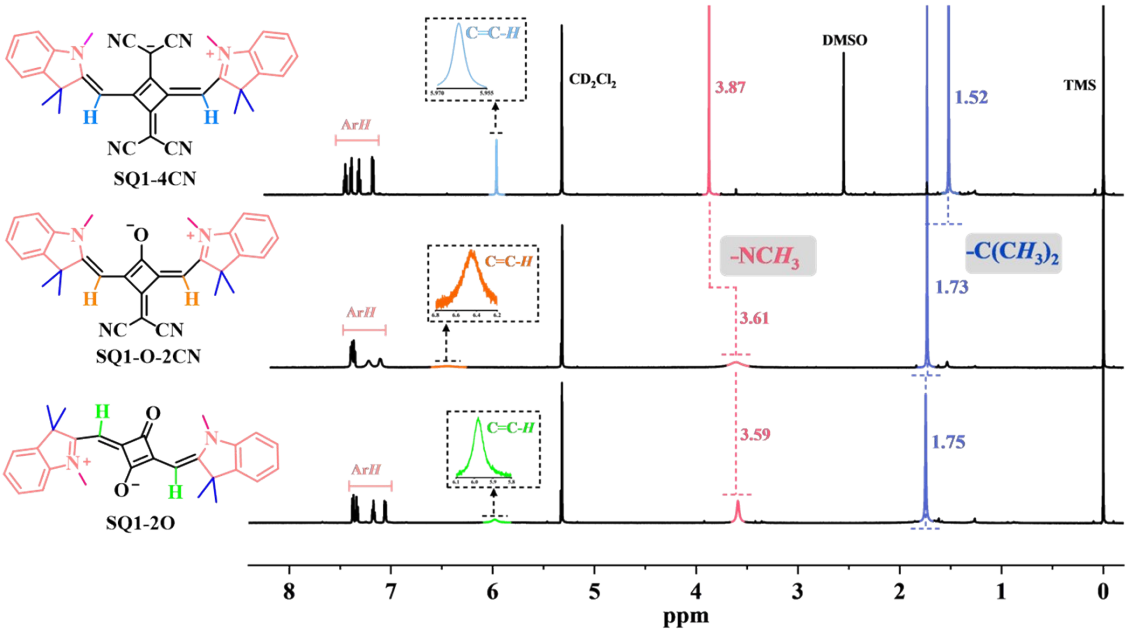

Fig. S1 Stacked ^{1}H NMR spectra of the SQ1 series in CD_2Cl_2.

3. Linear photophysical properties

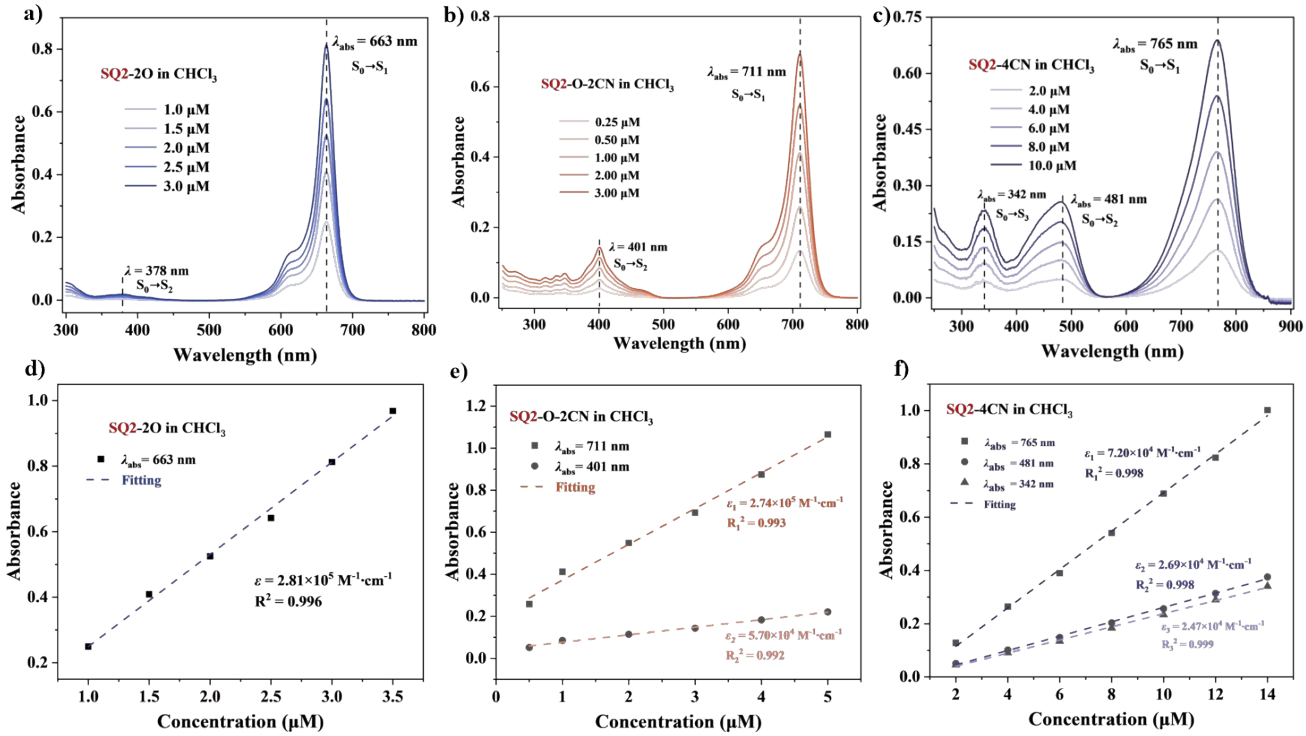

Fig. S2 Concentration effects of the dyes SQ2-2O (a), SQ2-O-2CN (b), and SQ2-4CN (c) in $CHCl_3$; Linear correlations of the absorbance intensity of SQ2-2O (d), SQ2-O-2CN (e), and SQ2-4CN (f) in $CHCl_3$.

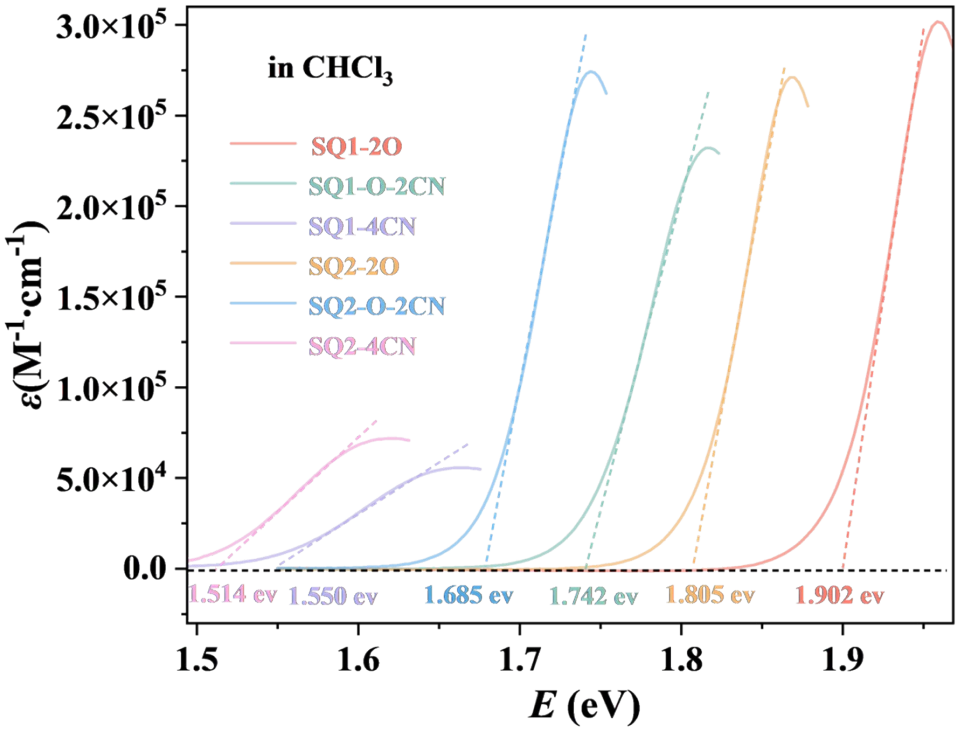

Fig. S3 Calculated optical bandgaps (E_g^{opt}) of the SQs in $CHCl_3$ at room temperature.

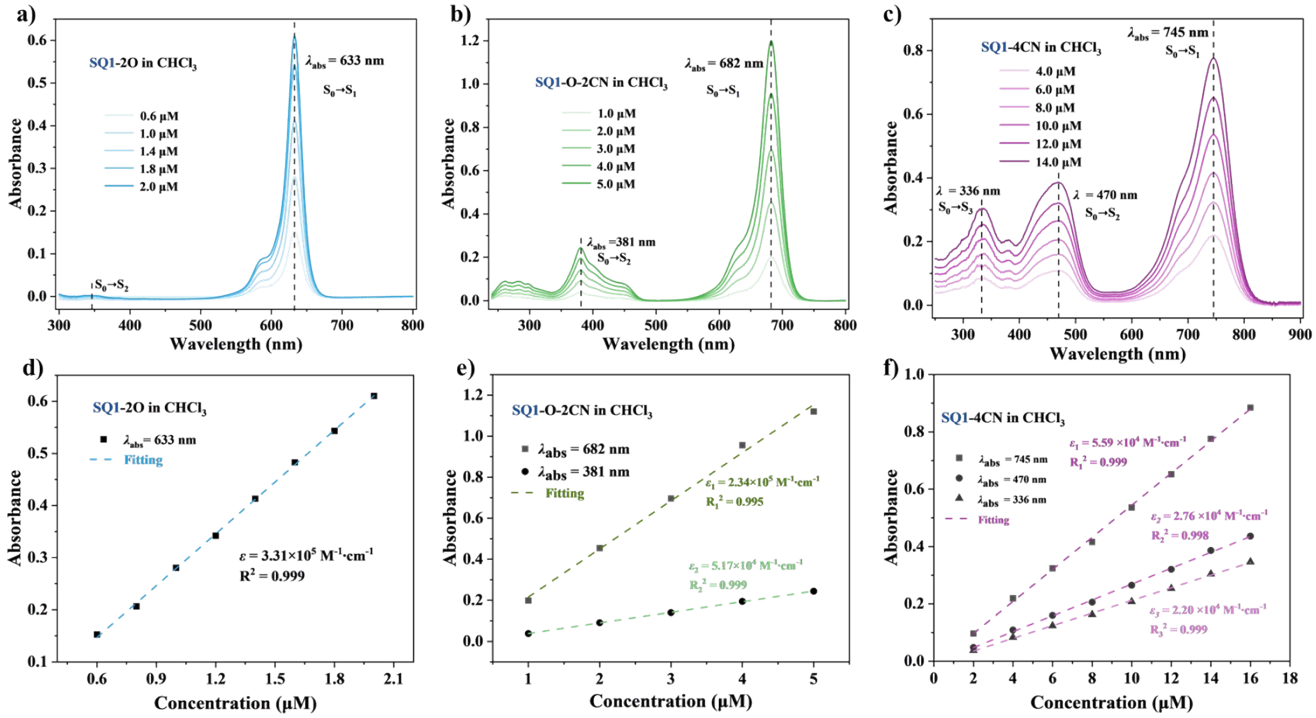

Fig. S4 Concentration effect of the dyes SQ1-2O (a), SQ1-O-2CN (b), and SQ1-4CN (c) in $CHCl_3$; Linear correlations of the absorbance intensity of SQ1-2O (d), SQ1-O-2CN (e), and SQ1-4CN (f) in $CHCl_3$.

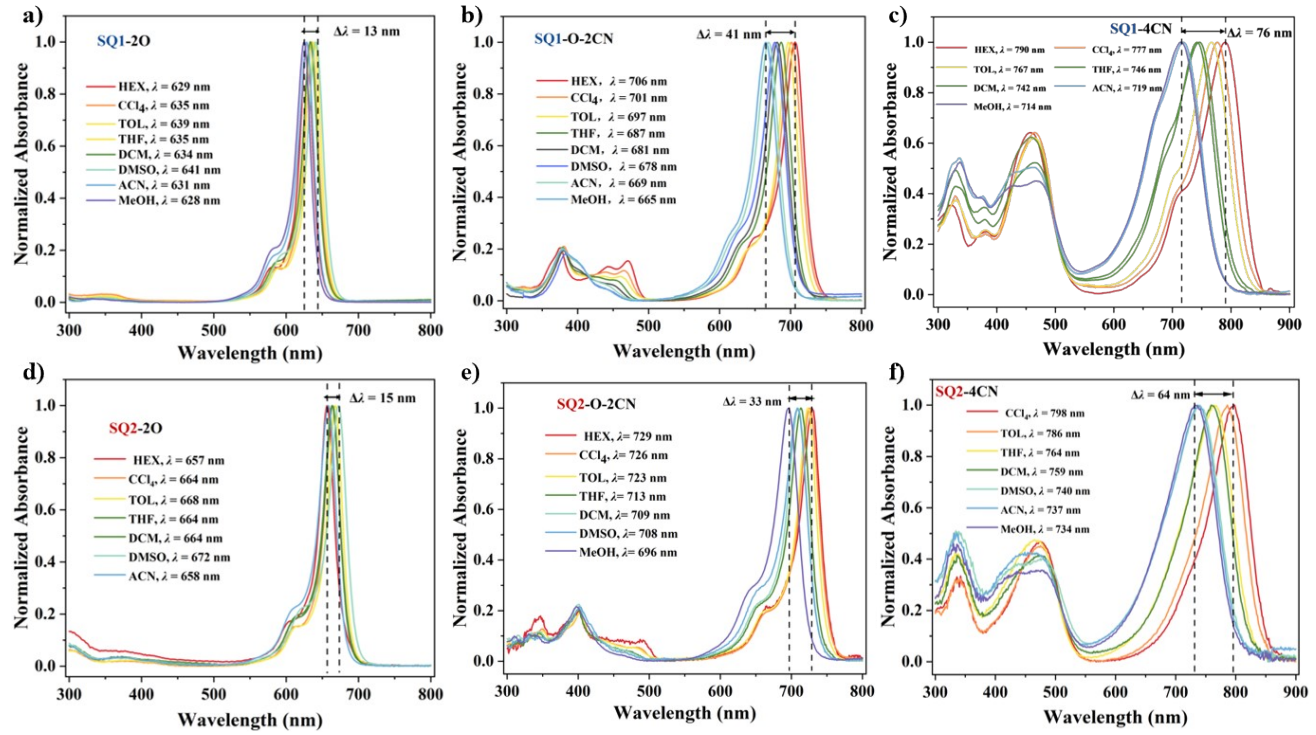

Fig. S5 Combined UV-vis absorption spectra of the dyes SQ1-2O (a), SQ1-O-2CN (b), SQ1-4CN (c), SQ2-2O (d), SQ2-O-2CN (e), and SQ2-4CN (f) in different solvents.

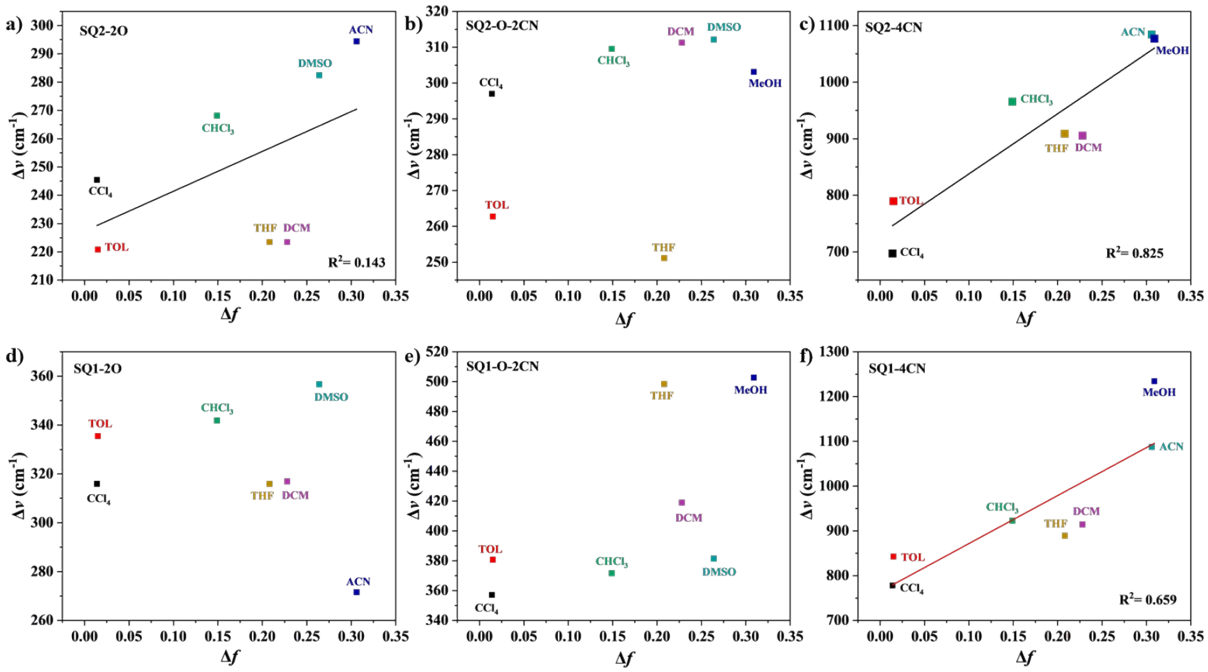

Fig. S6 Lippert-Mataga plots for the dyes SQ2-2O (a), SQ2-O-2CN (b), SQ2-4CN (c), SQ1-2O (d), SQ1-O-2CN (e), and SQ1-4CN (f) in different organic solvents.

Table S1 Summarized photophysical properties of the SQs in different organic solvents.

Solvents	Δf	SQ2-4CN			SQ1-4CN		
		λ_{abs} / nm	λ_{em} / nm	$\Delta\lambda$ / nm/cm^{-1}	λ_{abs} / nm	λ_{em} / nm	$\Delta\lambda$ / nm/cm^{-1}
CCl_4	0.014	798/473/342	845	47/697	777/464/330	827	50/778
TOL	0.015	786/475/342	838	52/789	767/465/331	820	53/843
$CHCl_3$	0.149	765/481/342	821	56/892	745/471/336	800	55/923
THF	0.208	764/472/334	826	62/983	746/458/330	799	53/889
DCM	0.228	759/480/336	815	56/905	742/465/329	796	54/914
ACN	0.306	737/471/335	801	64/1084	719/461/337	780	61/1088
MeOH	0.309	734/471/337	797	63/1077	714/471/337	783	69/1234
Solvents	Δf	**SQ2-O-2CN**			**SQ1-O-2CN**		
		λ_{abs} / nm	λ_{em} / nm	$\Delta\lambda$ / nm/cm^{-1}	λ_{abs} / nm	λ_{em} / nm	$\Delta\lambda$ / nm/cm^{-1}
CCl_4	0.014	726/403	742	16/297	701/380	719	18/357
TOL	0.015	723/402	737	14/263	697/380	716	19/381
$CHCl_3$	0.149	711/401	727	16/309	682/381	705	23/478
THF	0.208	713/399	726	13/251	687/378	706	19/392
DCM	0.228	709/401	725	16/311	681/380	701	20/419
DMSO	0.264	708/401	724	16/312	678/383	696	18/382
MeOH	0.309	696/397	711	15/303	665/380	688	23/503
Solvents	Δf	**SQ2-2O**			**SQ1-2O**		

		λ_{abs} / nm	λ_{em} / nm	$\Delta\lambda$ / nm/cm^{-1}	λ_{abs} / nm	λ_{em} / nm	$\Delta\lambda$ / nm/cm^{-1}
CCl_4	0.014	664	675	11/245	635	648	13/316
TOL	0.015	668	678	10/221	639	653	14/336
$CHCl_3$	0.149	663	675	12/268	633	647	14/342
THF	0.208	664	674	10/223	635	648	13/316
DCM	0.228	664	674	10/223	634	647	13/317
DMSO	0.264	672	685	13/282	641	656	15/357
ACN	0.306	658	671	13/295	631	642	11/272

Notes: All the data were obtained experimentally.

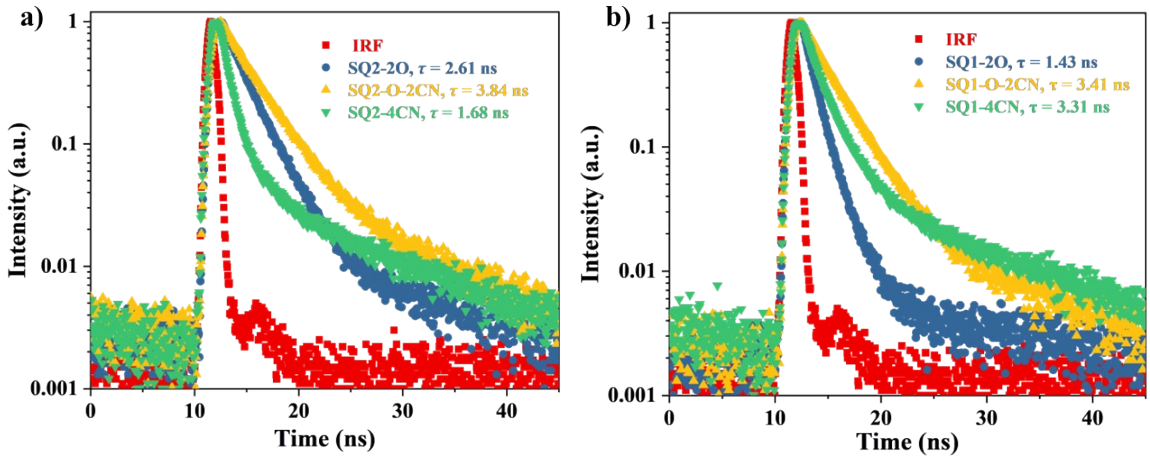

Fig. S7 Fluorescence decay curves of the SQ2 series (a) and the SQ1 series (b) in $CHCl_3$.

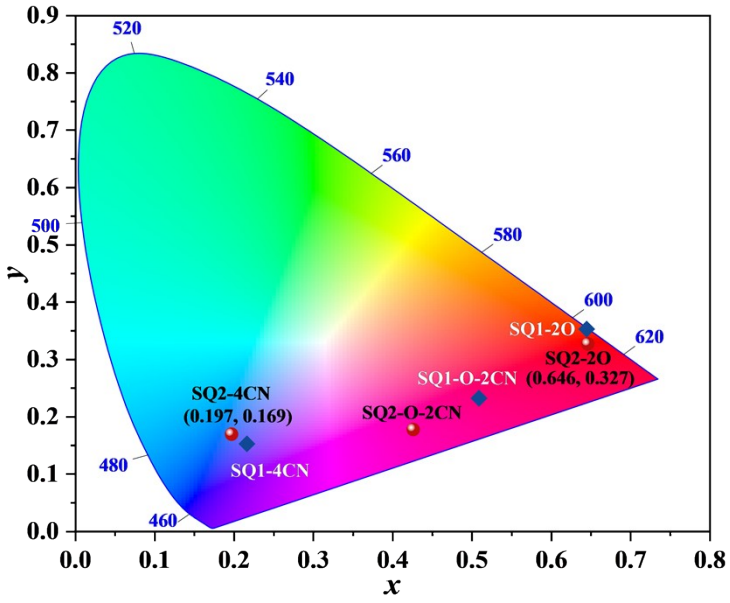

Fig. S8 Plotted CIE 1931 chromaticity diagram based on the UV-vis absorption maxima of both SQs series in $CHCl_3$.

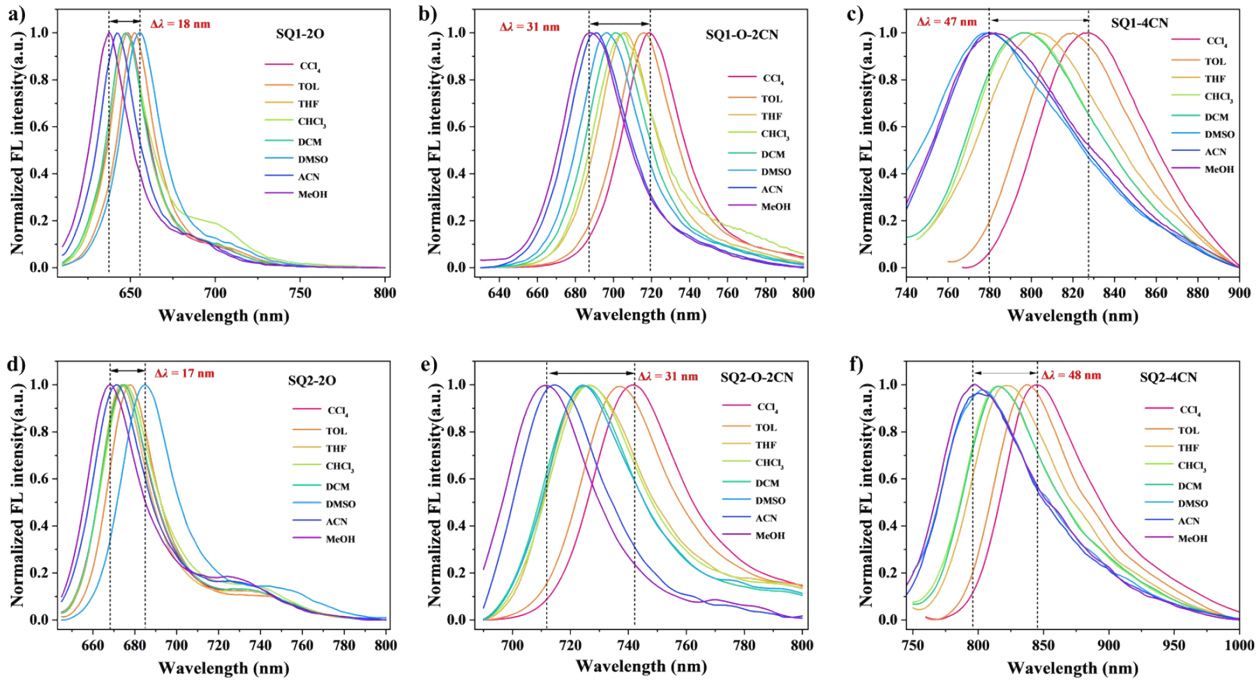

Fig. S9 Normalized fluorescence emission spectra of the SQ1-2O (a), SQ1-O-2CN (b), SQ1-4CN (c), SQ2-2O (d), SQ2-O-2CN (e), and SQ2-4CN (f) in different organic solvents.

Table S2 Summarized photophysical properties of the investigated SQ1 series.

Dyes [a]	λ_{abs}	ε	λ_{em}	$\Delta\lambda$	FWHM	Φ_F	τ_F	E_g^{opt} [b]	$\Delta\mu_{01}$ [c]
	nm	$M^{-1}\cdot cm^{-1}$	nm	nm	nm		ns	eV	D
SQ1-2O	633	3.31×10^5	647	14	24	18.6%	1.43	1.902	12.24
SQ1-O-2CN	682	2.34×10^5	700	18	36	28.9%	3.41	1.742	12.62

[a] in $CHCl_3$; [b] E_g^{opt} (eV) = $1240/\lambda_{edg}$; [c] $\mu_{01} = 0.09584 \times \sqrt{\int \frac{\varepsilon(\nu)}{\nu^{max}} d\nu}$

4. Quantum chemical calculations

Density functional theory (DFT) under the CAM-B3LYP/6-311G (d,p) level in vacuum was used to investigate the quantum chemical properties of the investigated squaraines in this work.[8,9] A conformational screening was performed for all the molecular structures. To be noted, the *cis*-conformations for the SQ1-O-2CN and SQ2-O-2CN were evaluated following the reported crystallographic data.[10,11] Electron excitation analysis was conducted through time-dependent DFT (TD-DFT). All DFT and TD-DFT calculations were performed using Gaussian 09W. Multiwfn was used in the wave function analysis.[12]

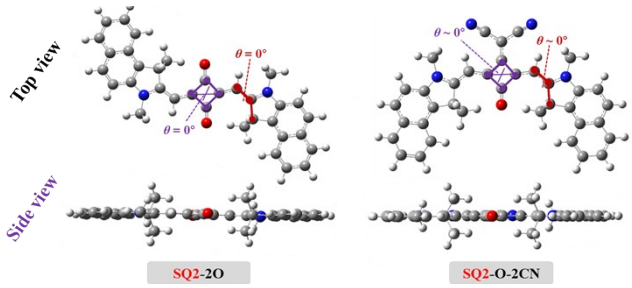

Fig. S10 Optimized geometries and dihedral angles of the dyes SQ2-2O and SQ2-O-2CN in their ground states.

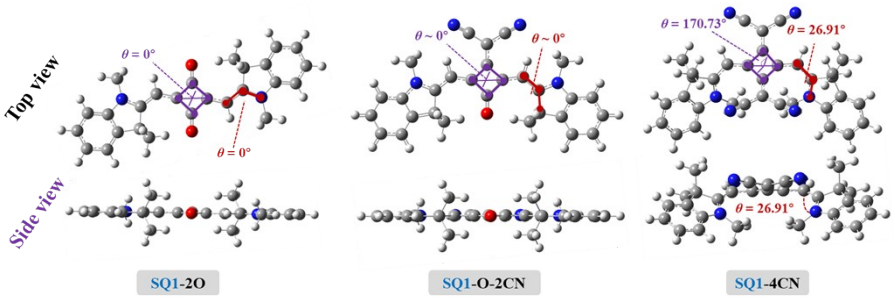

Fig. S11 Optimized geometries and dihedral angles of the SQ1 dyes in their ground states.

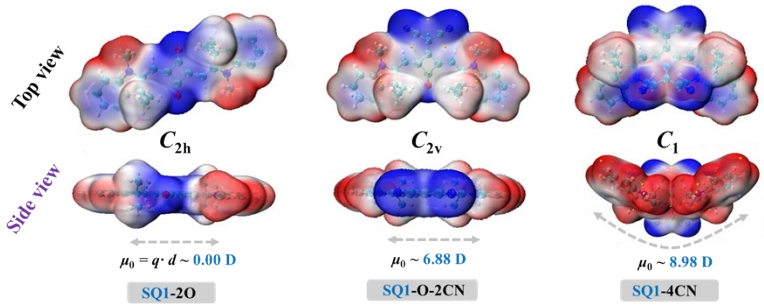

Fig. S12 Electrostatic potential map of the dyes SQ1-2O, SQ1-O-2CN, and SQ1-4CN.

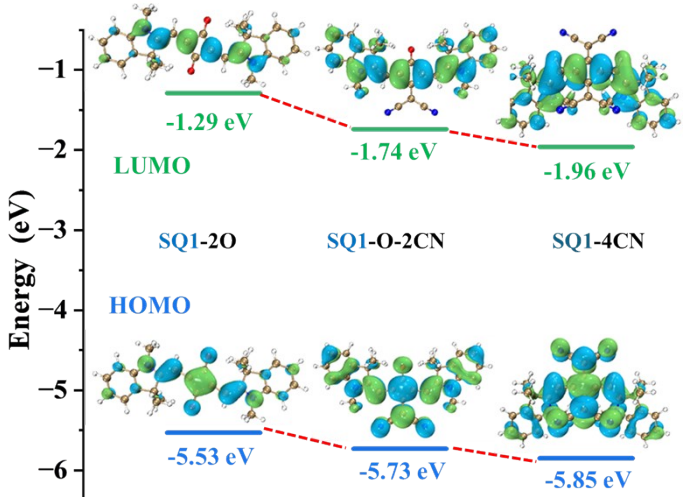

Fig. S13 Frontier molecular orbitals and energy levels from the DFT calculations of SQ1 series.

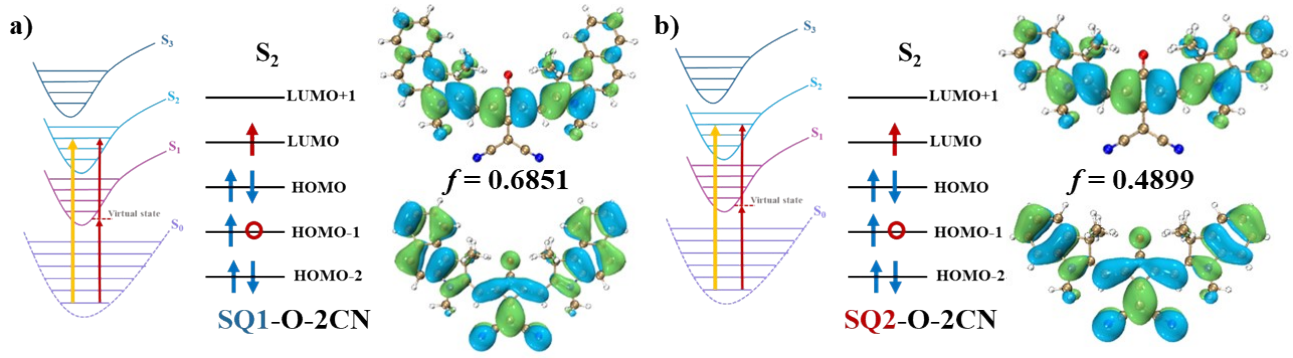

Fig. S14 High-order absorption band orbital transition contributions in SQ1-O-2CN (a) and SQ2-O-2CN (b).

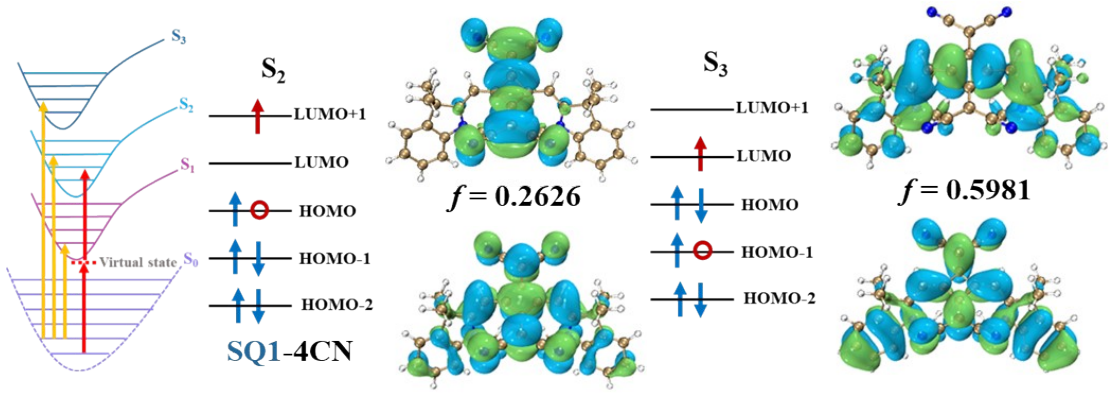

Fig. S15 High-order absorption band orbital transition contributions in SQ1-4CN.

Table S3 Excited states, symmetry, transitions, and oscillator strength of SQs.

Excited State	Symmetry	SQ2-4CN		SQ1-4CN	
		Transitions	Osc. Strength	Transitions	Osc. Strength
S_1	Singlet-A	H → L (98.0%)	0.6083	H → L (98.6%)	0.4455
S_2	Singlet-A	H → L+1 (94.0%)	0.2294	H → L+1 (94.6%)	0.2626
S_3	Singlet-A	H-1 → L (82.3%)	0.6953	H-1 → L (93.2%)	0.5981
Excited State	**Symmetry**	**SQ2-O-2CN**		**SQ1-O-2CN**	
		Transitions	**Osc. Strength**	**Transitions**	**Osc. Strength**
S_1	Singlet-A	H → L (97.4%)	0.9361	H → L (97.8%)	0.8623
S_2	Singlet-A	H-1 → L (86.4%)	0.4899	H-1 → L (93.9%)	0.6851
Excited State	**Symmetry**	**SQ2-2O**		**SQ1-2O**	
		Transitions	**Osc. Strength**	**Transitions**	**Osc. Strength**
S_1	Singlet-A	H → L (97.6%)	1.5523	H → L (98.3%)	1.4412

5. Two-photon absorption (2PA) properties

2PA measurements were conducted following the procedures which were introduced in our previous reports.[13,14] By referencing the known 2PA cross section of Rhodamine B (~53 GM at 650 nm) listed in the literature, each measurement was repeated multiple times and averaged to retrieve the NLO coefficients.[15]

Table S4 Corresponding δ_{2PA} values of SQ2-4CN excited with different femtosecond wavelengths.

λ/nm	δ_{2PA}/GM	λ/nm	δ_{2PA}/GM	λ/nm	δ_{2PA}/GM
880	1877	920	853	960	741
890	**2140**	930	1123	970	753
900	1437	940	1072	980	607
910	1450	950	710	1000	365

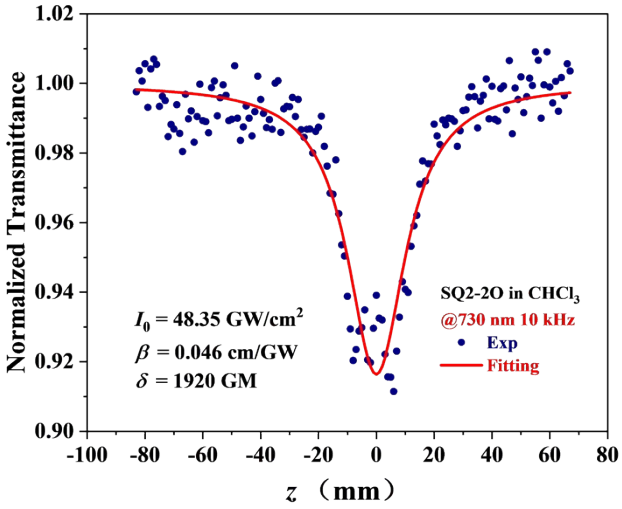

Fig. S16 Normalized transmittance curves and δ_{2PA} values of SQ2-2O in $CHCl_3$.

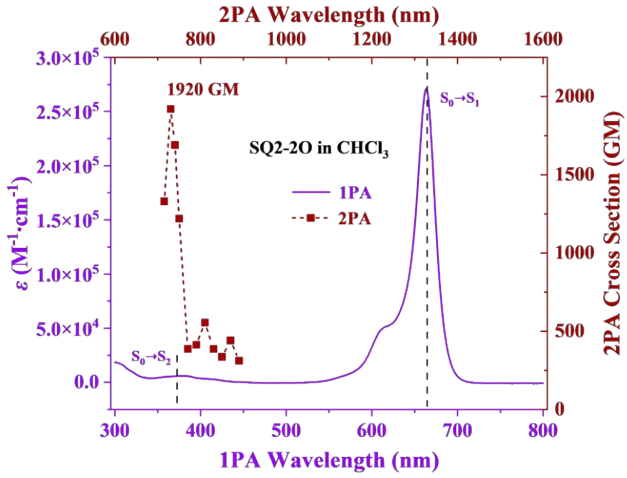

Fig. S17 Combined 1PA and 2PA spectra of the dye SQ2-2O in $CHCl_3$.

Table S5 Corresponding δ_{2PA} values of SQ2-2O excited with different femtosecond wavelengths.

λ/nm	δ_{2PA}/GM	λ/nm	δ_{2PA}/GM	λ/nm	δ_{2PA}/GM
715	1330	790	414	870	441
730	**1920**	810	555	890	312
750	1220	830	387	---	---
770	388	850	337	---	---

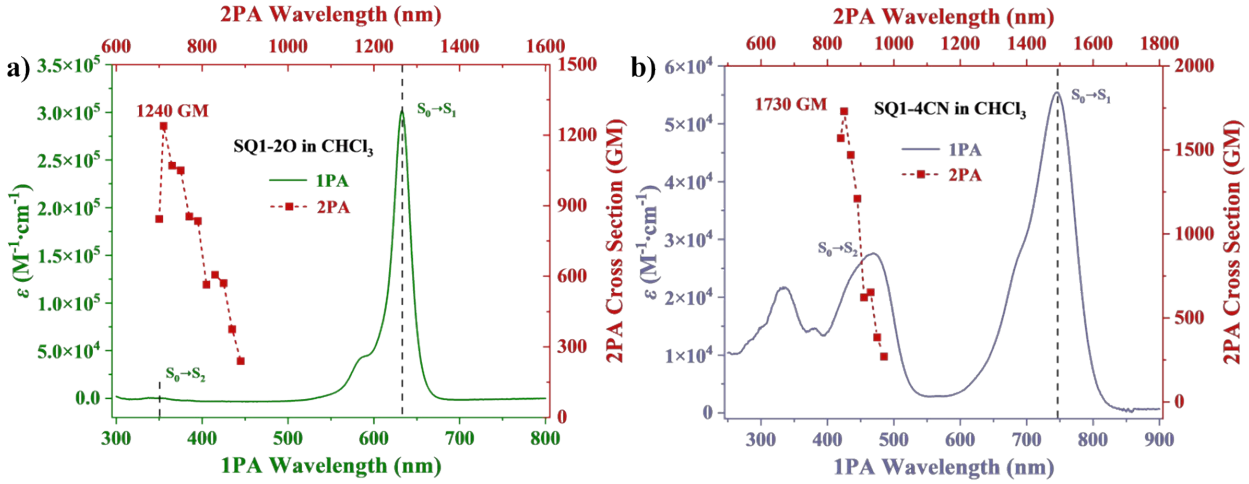

Fig. S18 Combined 1PA and 2PA spectra of the dyes SQ1-2O (a) and SQ1-4CN (b) in $CHCl_3$.

Table S6 Corresponding δ_{2PA} values of SQ1-2O excited with different femtosecond wavelengths.

λ/nm	δ_{2PA}/GM	λ/nm	δ_{2PA}/GM	λ/nm	δ_{2PA}/GM
700	844	770	854	850	571
710	**1240**	790	835	870	375
730	1070	810	564	890	239
750	1050	830	606	-	-

Table S7 Corresponding δ_{2PA} values of SQ1-4CN excited with different femtosecond wavelengths.

λ/nm	δ_{2PA}/GM	λ/nm	δ_{2PA}/GM
840	1570	910	622
850	**1730**	930	652
870	1470	950	384
890	1210	970	270

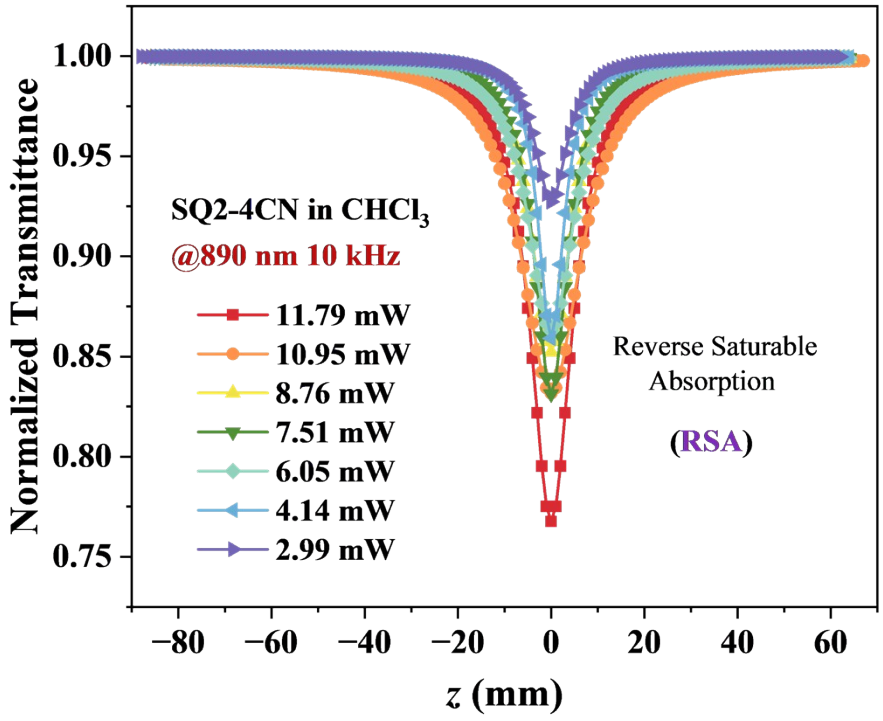

Fig. S19 Normalized transmittance curves of SQ2-4CN in $CHCl_3$ excited at 890 nm under various laser input intensities.

6. Femtosecond transient absorption (fs-TA) spectroscopy

The fs-TA setup used for this work was based on a PHAROS laser system with Light Conversion (1030 nm, 200 fs, 200 μJ/pulse, and 100 kHz repetition rate), nonlinear frequency mixing techniques and the Femto-TA100 spectrometer. The experimental details have been comprehensively elaborated in previous literature.[16]

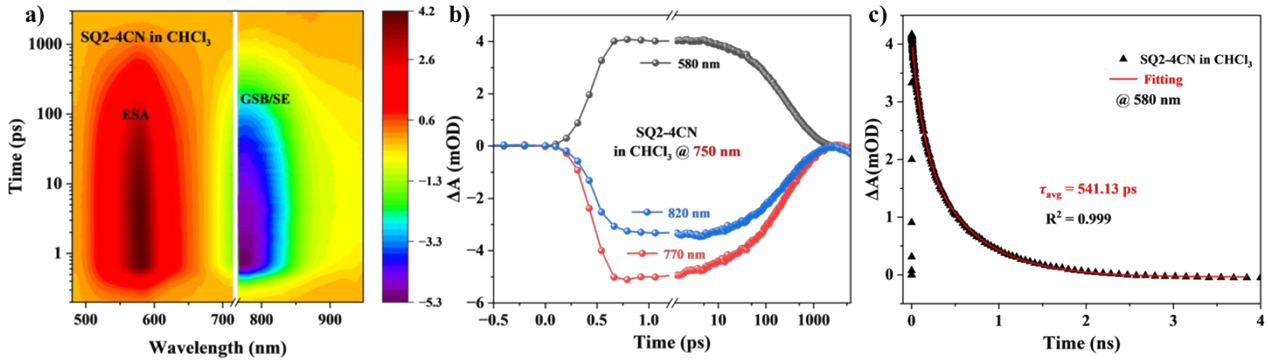

Fig. S20 (a) 2D contour map of the fs-TA spectra of SQ2-4CN in $CHCl_3$ at fs-750 nm; (b) Upon photoexcitation of SQ2-4CN in $CHCl_3$ excited at fs-750 nm, plots of selected kinetic traces superimposed with matching curves at different wavelengths; (c) Related decay curves of SQ2-4CN at 580 nm.

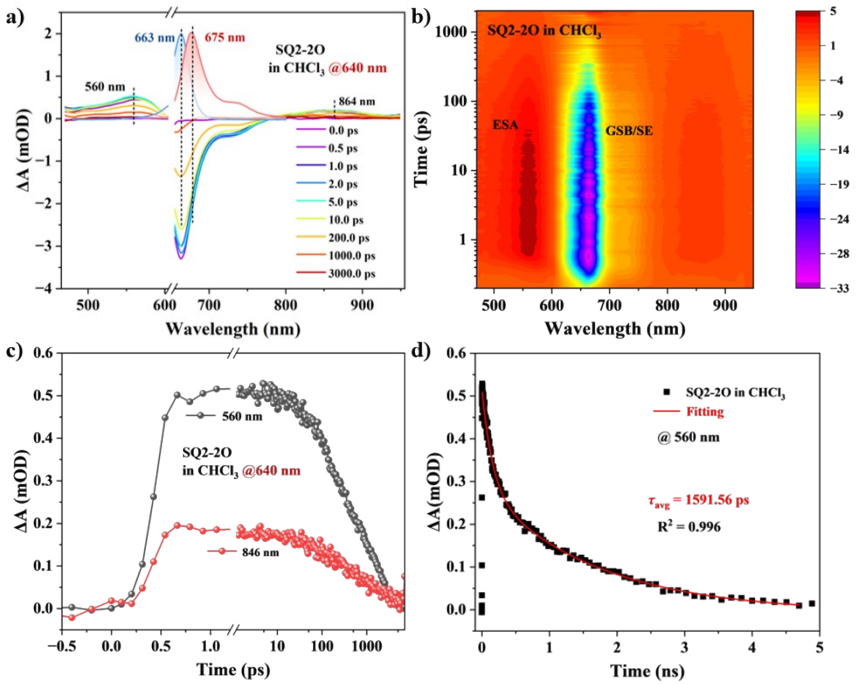

Fig. S21 (a) fs-TA delay spectra of SQ2-2O excited at fs-640 nm; (b) 2D contour map of the fs-TA spectra of SQ2-2O; (c) Upon photoexcitation of SQ2-2O in $CHCl_3$ excited at fs-640 nm, plots of selected kinetic traces superimposed with matching curves at different wavelengths; (d) Related decay curves of SQ2-2O at 560 nm.

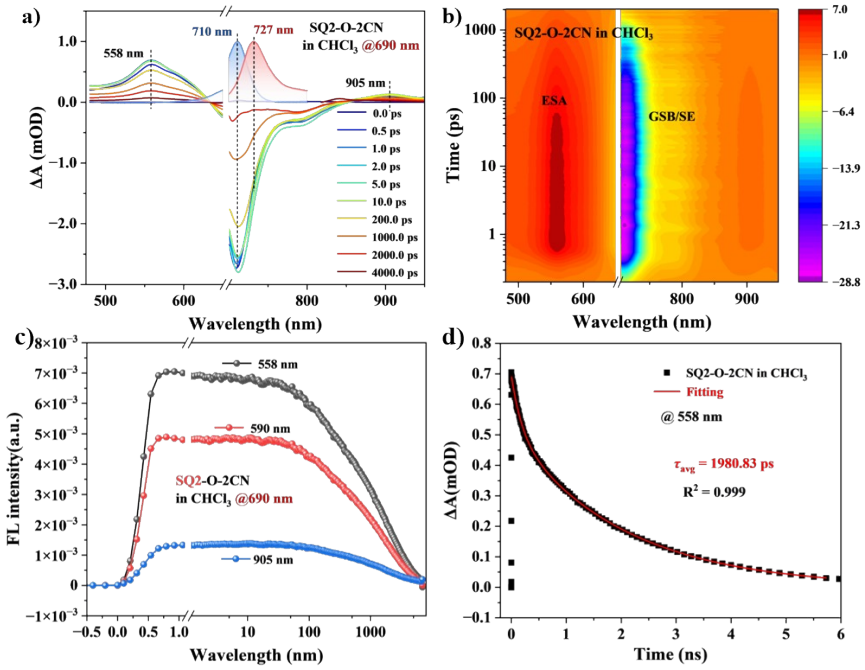

Fig. S22 (a) fs-TA delay spectra of SQ2-O-2CN excited at fs-690 nm; (b) 2D contour map of the fs-TA spectra of SQ2-O-2CN; (c) Upon photoexcitation of SQ2-O-2CN in $CHCl_3$ excited at fs-690 nm, Plots of selected kinetic traces superimposed with matching curves at different wavelengths; (d) Related decay curves of SQ2-O-2CN at 558 nm.

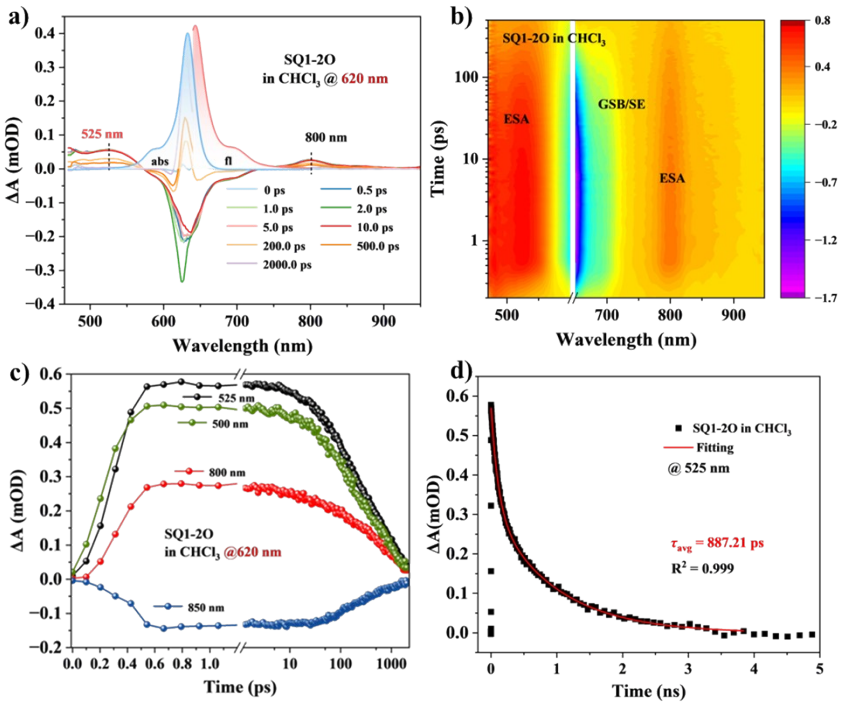

Fig. S23 (a) fs-TA delay spectra of SQ1-2O excited at fs-620 nm; (b) 2D contour map of the fs-TA spectra of SQ1-2O; (c) Upon photoexcitation of SQ1-2O in $CHCl_3$ excited at fs-620 nm, plots of selected kinetic traces superimposed with matching curves at different wavelengths; (d) Related decay curves of SQ1-2O at 525 nm.

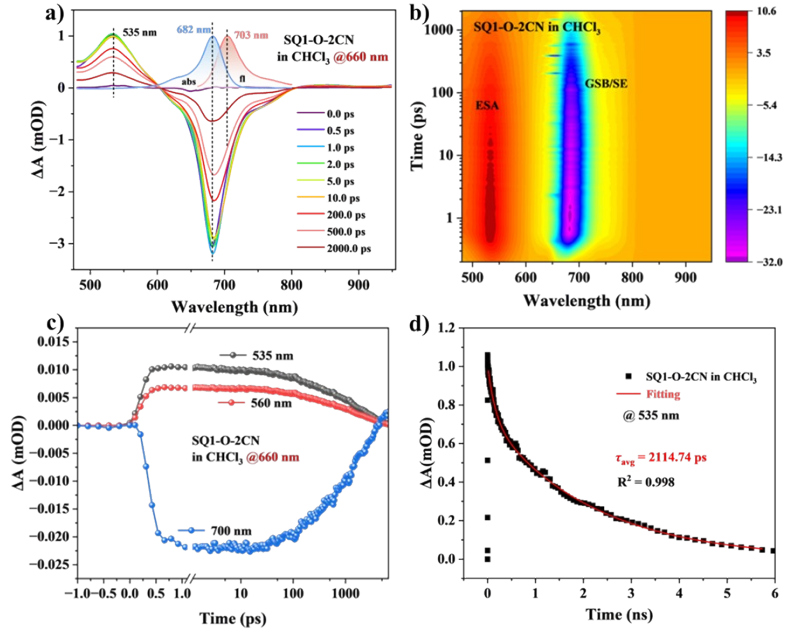

Fig. S24 (a) fs-TA delay spectra of SQ1-O-2CN excited at fs-660 nm; (b) 2D contour map of the fs-TA spectra of SQ1-O-2CN; (c) Upon photoexcitation of SQ1-O-2CN in $CHCl_3$ excited at fs-660 nm, Plots of selected kinetic traces superimposed with matching curves at different wavelengths; (d) Related decay curves of SQ1-O-2CN at 535 nm.

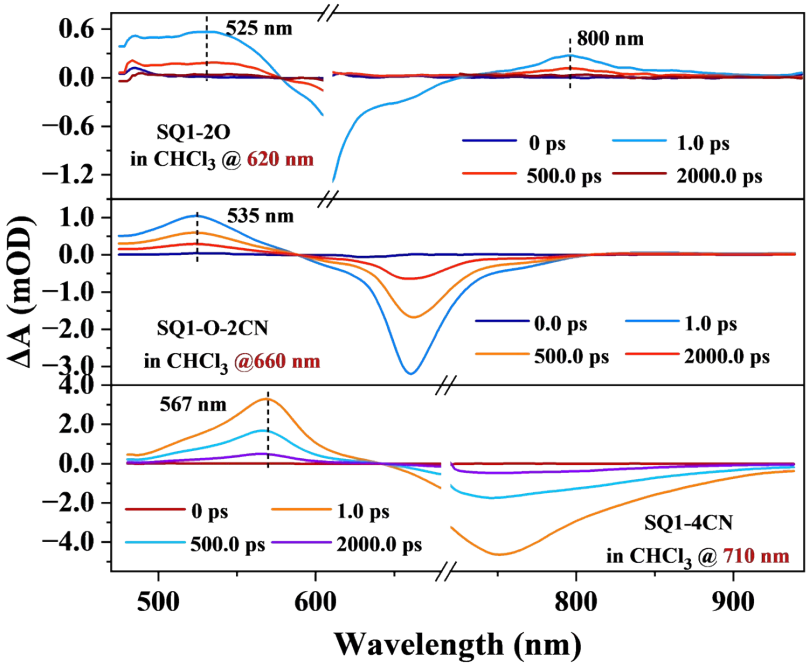

Fig. S25 fs-TA delay spectra of SQ1 dyes in $CHCl_3$.

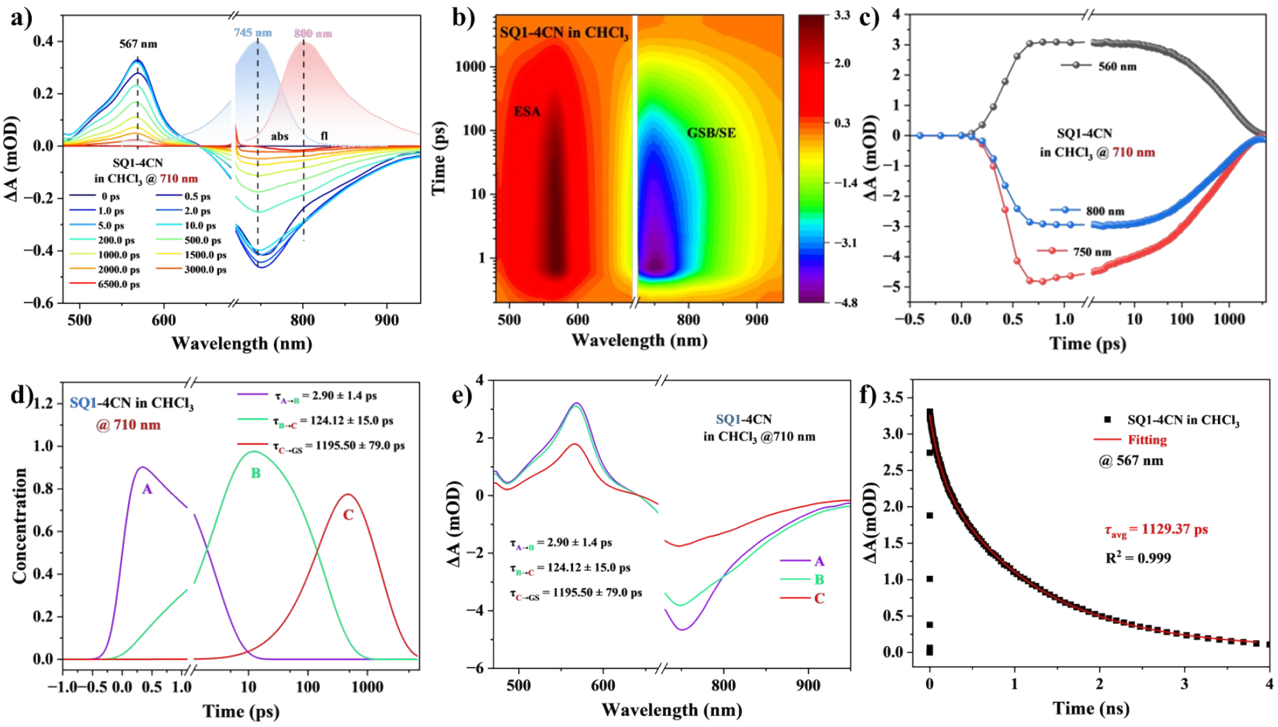

Fig. S26 (a) fs-TA delay spectra of SQ1-4CN excited at fs-710 nm in $CHCl_3$; (b) 2D contour map of the fs-TA spectra of SQ1-4CN; (c) Upon photoexcitation of SQ1-4CN in $CHCl_3$ excited at fs-710 nm, plots of selected kinetic traces superimposed with matching curves at different wavelengths; (d) Species-associated spectra plots and (e) kinetic model plots of SQ1-4CN in $CHCl_3$ excited at fs-710 nm; (f) Decay curves of SQ1-4CN excited state signals at 567 nm.

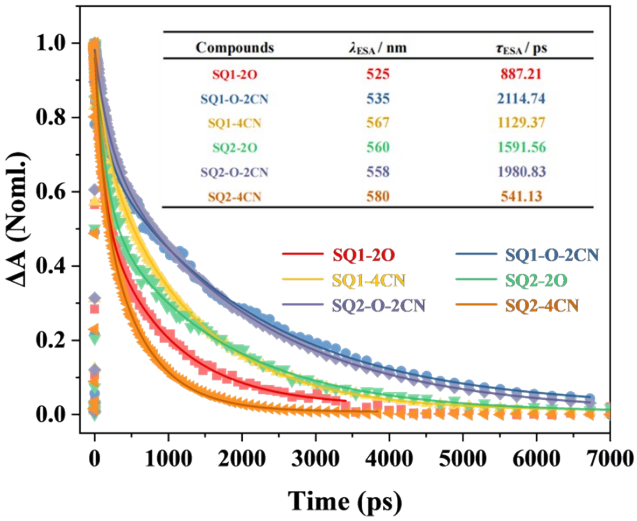

Fig. S27 Normalized ESA kinetics of SQ1 series and SQ2 series.

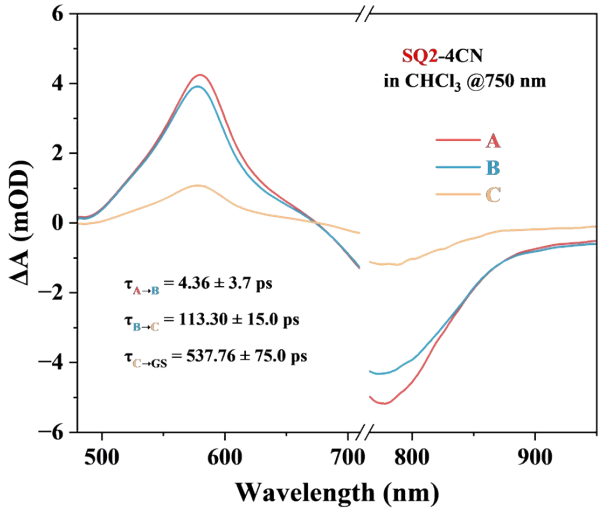

Fig. S28 Species-associated spectra plots of SQ2-4CN in $CHCl_3$ excited at fs-750 nm.

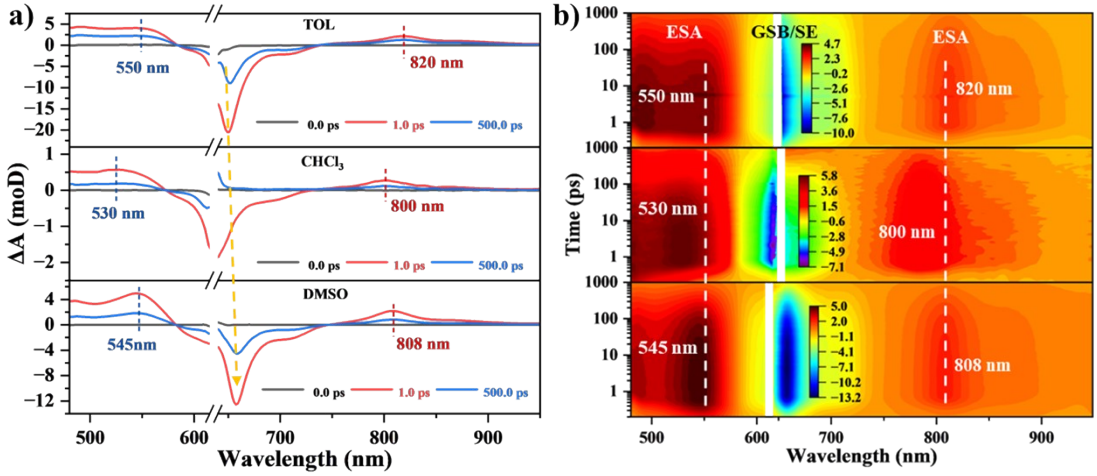

Fig. S29 fs-TA spectra (a) and related 2D contour map (b) of the fs-TA spectra of SQ1-2O in TOL, $CHCl_3$, and DMSO.

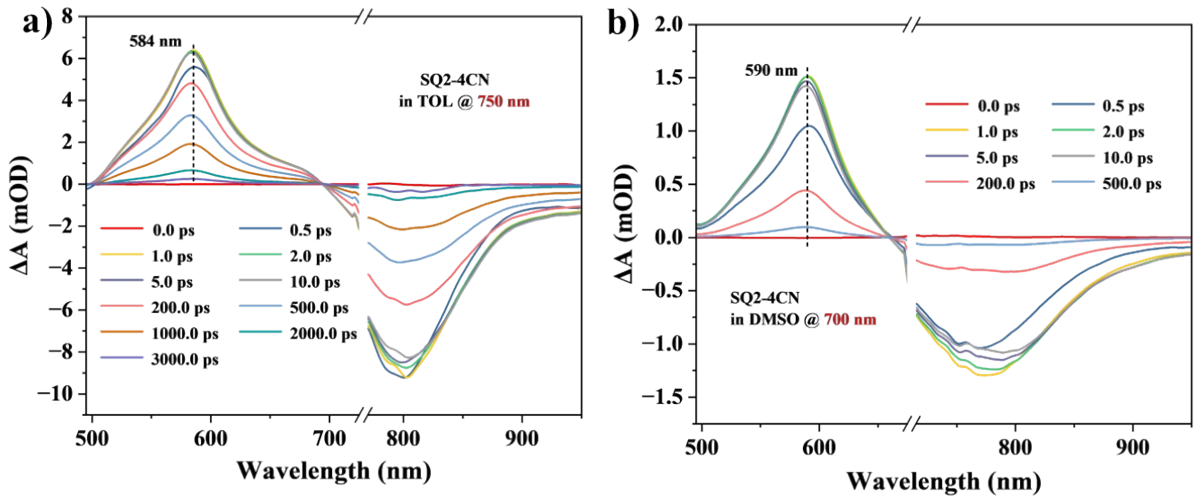

Fig. S30 fs-TA delay spectra of SQ2-4CN excited at fs-750 nm in TOL (a) and fs-700 nm in DMSO (b).

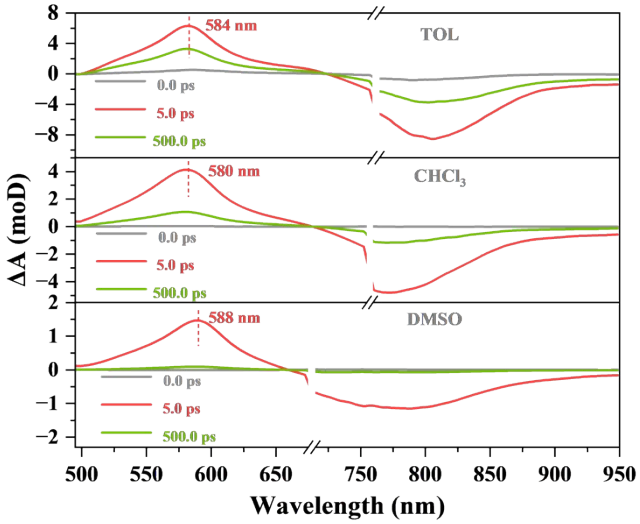

Fig. S31 fs-TA spectra of SQ2-4CN in TOL, $CHCl_3$, and DMSO.

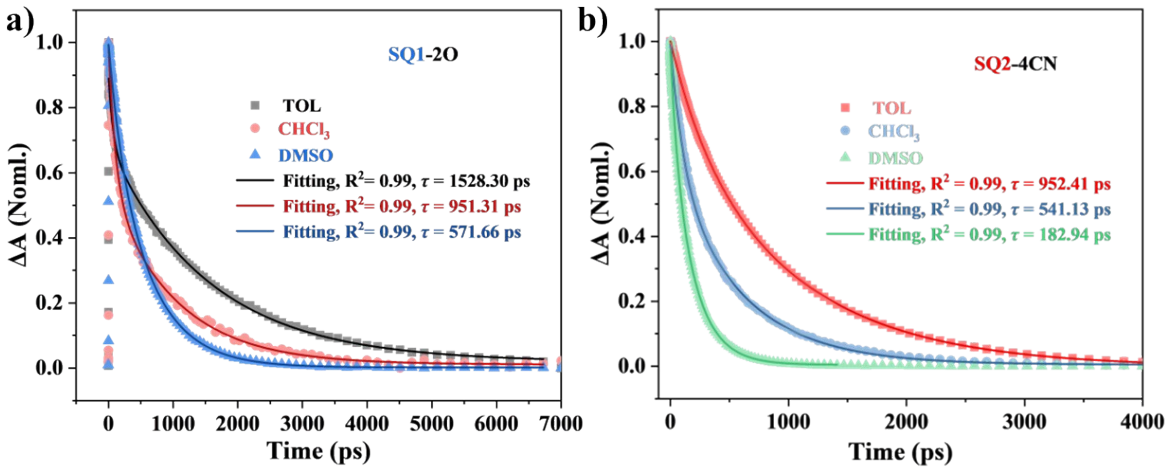

Fig. S32 Normalized ESA kinetics of SQ1-2O (a) and SQ2-4CN (b) in TOL, $CHCl_3$, and DMSO.

Table S8 ESA decay lifetimes and fluorescence quantum yields of SQ2-4CN in TOL, $CHCl_3$, and DMSO.

Solvents	TOL	$CHCl_3$	DMSO
τ / ps	952.41	541.13	182.94
Φ_F	5.4%	3.5%	0.9%

7. Photothermal conversion and antibacterial capacity determination

The photothermal conversion efficiency of SQs was determined by measuring the temperature change of SQs in the DMSO/water solution (1/9, *v*/*v*) as a function of time under the continuous irradiation of 808 nm laser for 10 min (*t*) till the temperature of solution reached a steady-state case. The photothermal conversion efficiency (η) was calculated based on the following Eq. S1.

$$\eta = [\, hA\,(T_{max} - T_{sur}) - Q_{dis}] \,/\, [\, I\,(1 - 10^{-A_{808}})\,] \qquad \text{(S1)}$$

Here, h is the heat transfer coefficient, A is the surface area of the container, T_{max} is the maximum steady-state temperature, T_{sur} is the ambient temperature of the environment, Q_{dis} is the heat dissipation from the light absorbed by the solvent and the quartz sample cell, I is the incident laser power, and A_{808} is the absorbance of the sample at 808 nm (0.15, 1.0 mm cuvette). The value of hA is calculated based on the following Eq. S2.

$$hA = m_D \cdot c_D / \tau_s \qquad \text{(S2)}$$

Here, τ_s is the time constant for the heat transfer in the system (τ_s = 215.88 s), and m_D and c_D are the mass (1.0 g) and heat capacity (3.975 J/g/°C) of the solvent mixture (DMSO/water = 1/9), respectively. The hA was determined to be 18.4 mW/°C. The calculated photothermal conversion efficiency of SQ2-4CN in the DMSO/water solution was ~ 42.4%.

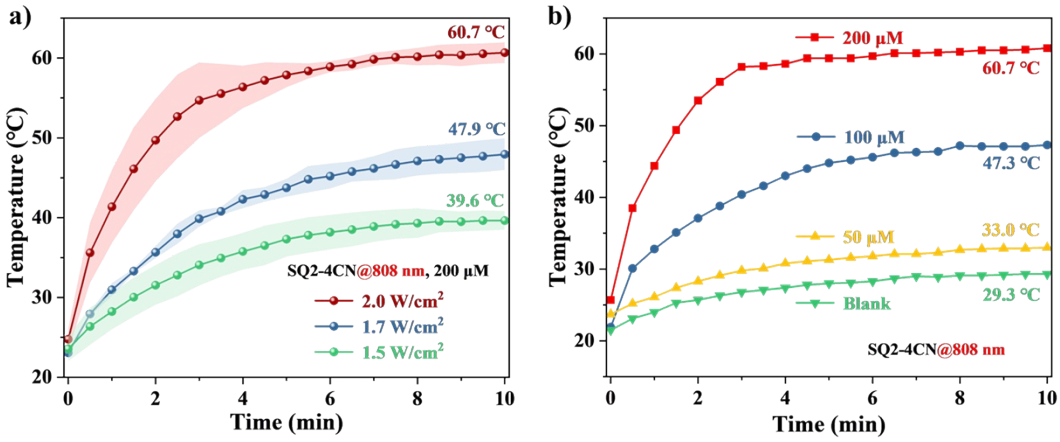

Fig. S33 (a) Temperature effect under continuous 808 nm laser irradiation for 10 min with different laser power densities [SQ2-4CN in the DMSO/water solution (1/9, *v*/*v*), 200 μM]; (b) Temperature effect under continuous 808 nm laser irradiation for 10 min with different concentrations at 2.0 W/cm^2 [SQ2-4CN in the DMSO/water solution (1/9, *v*/*v*)].

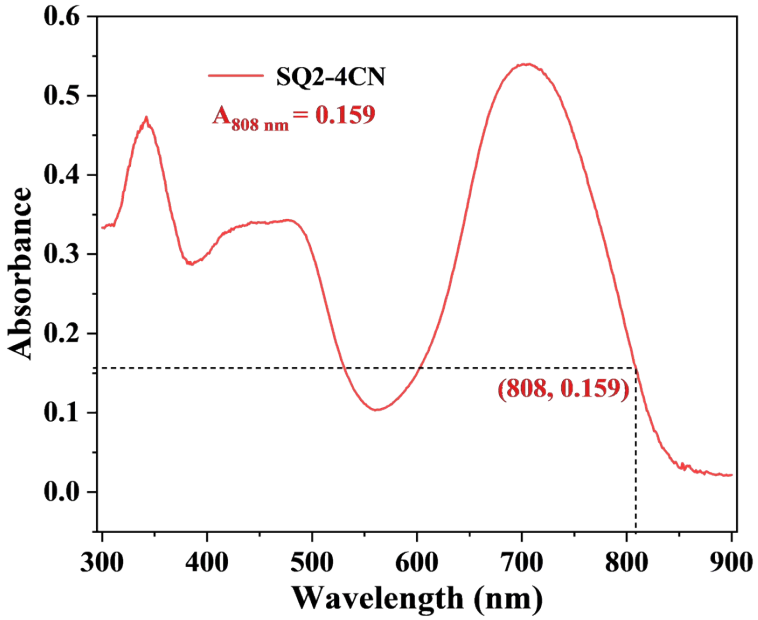

Fig. S34 UV-vis spectrum of SQ2-4CN in the DMSO/water solution (1/9, *v*/*v*). *Notes:* $c_{SQ2\text{-}4CN}$ = 200.0 μM.

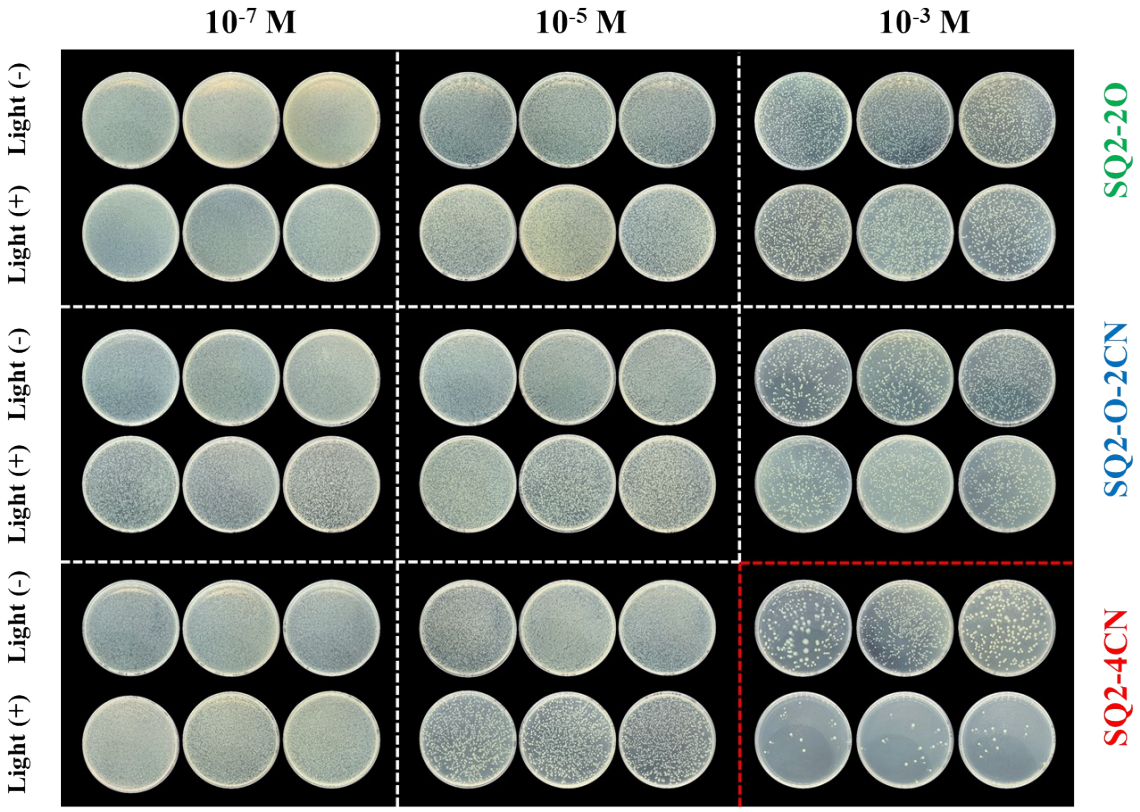

Fig. S35 Comparative images depicting the effects of 808 nm laser irradiation on *E. coli* colonies from triplicate parallel experiments with varying concentrations of the SQ2s dyes.

8. NMR spectra of the dyes

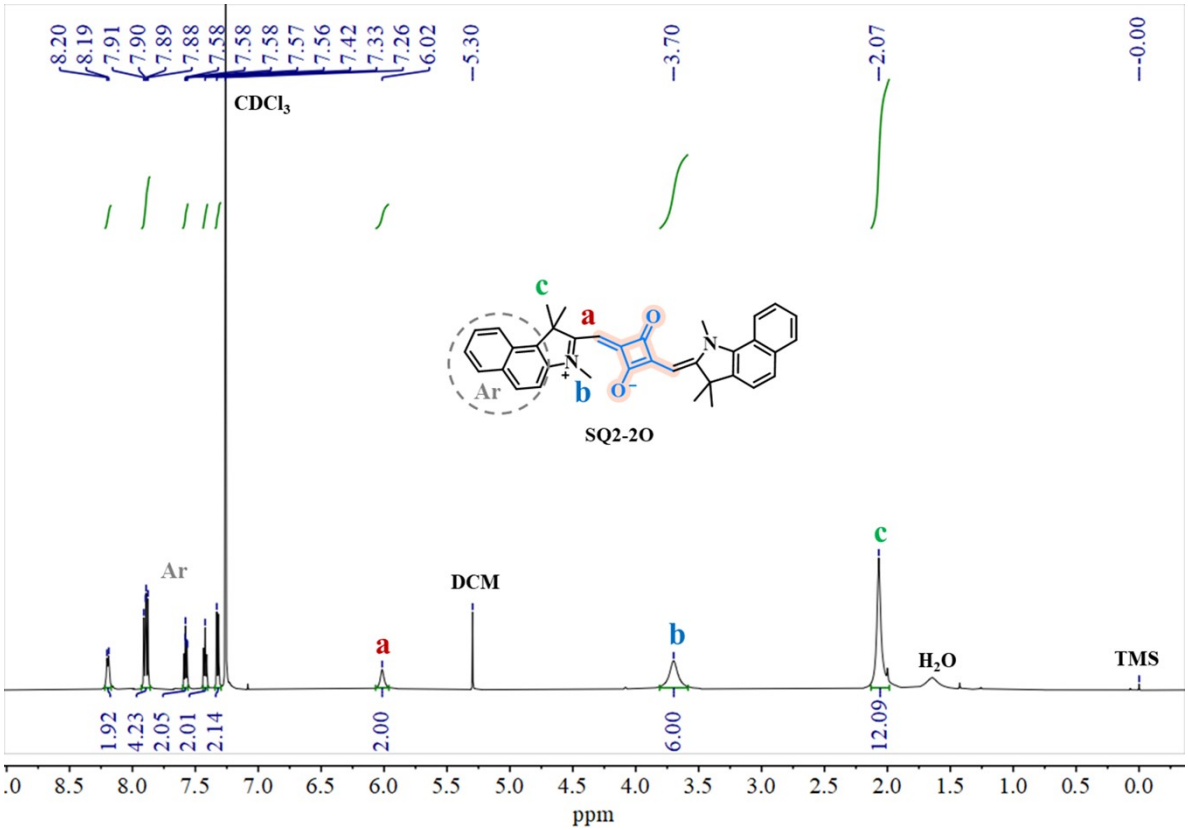

Fig. S36 ^{1}H NMR spectrum of the dye SQ2-2O in $CDCl_3$.

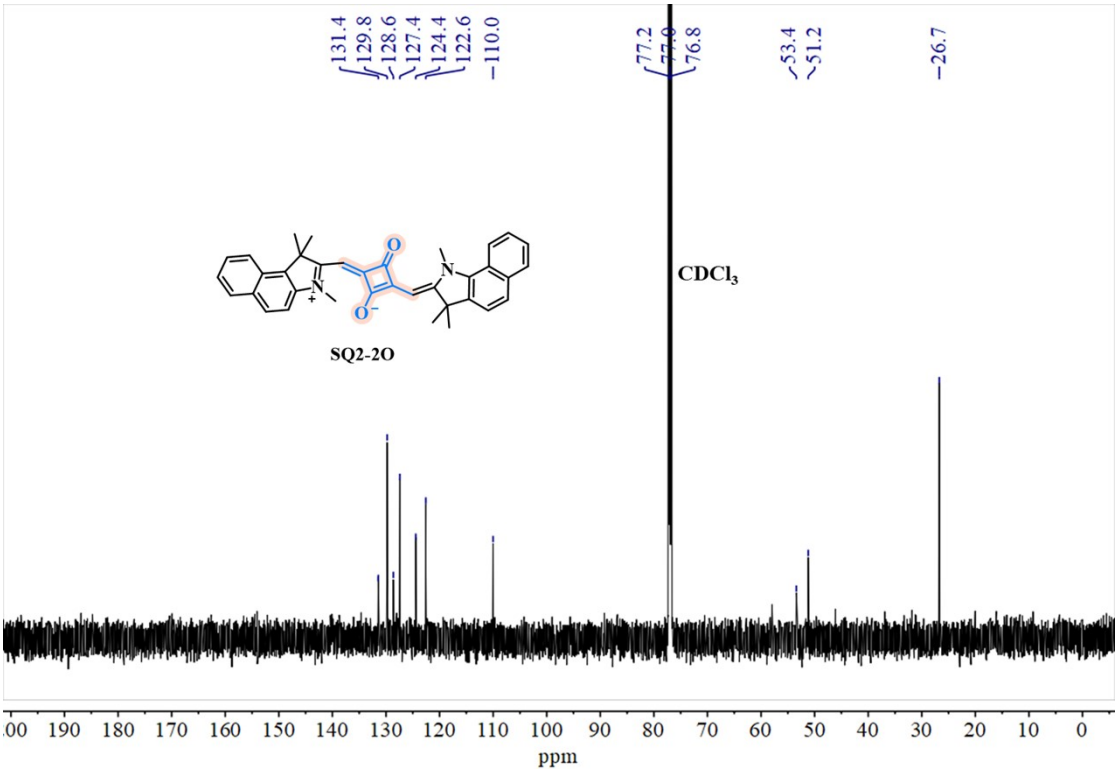

Fig. S37 ^{13}C NMR spectrum of the dye SQ2-2O in $CDCl_3$.

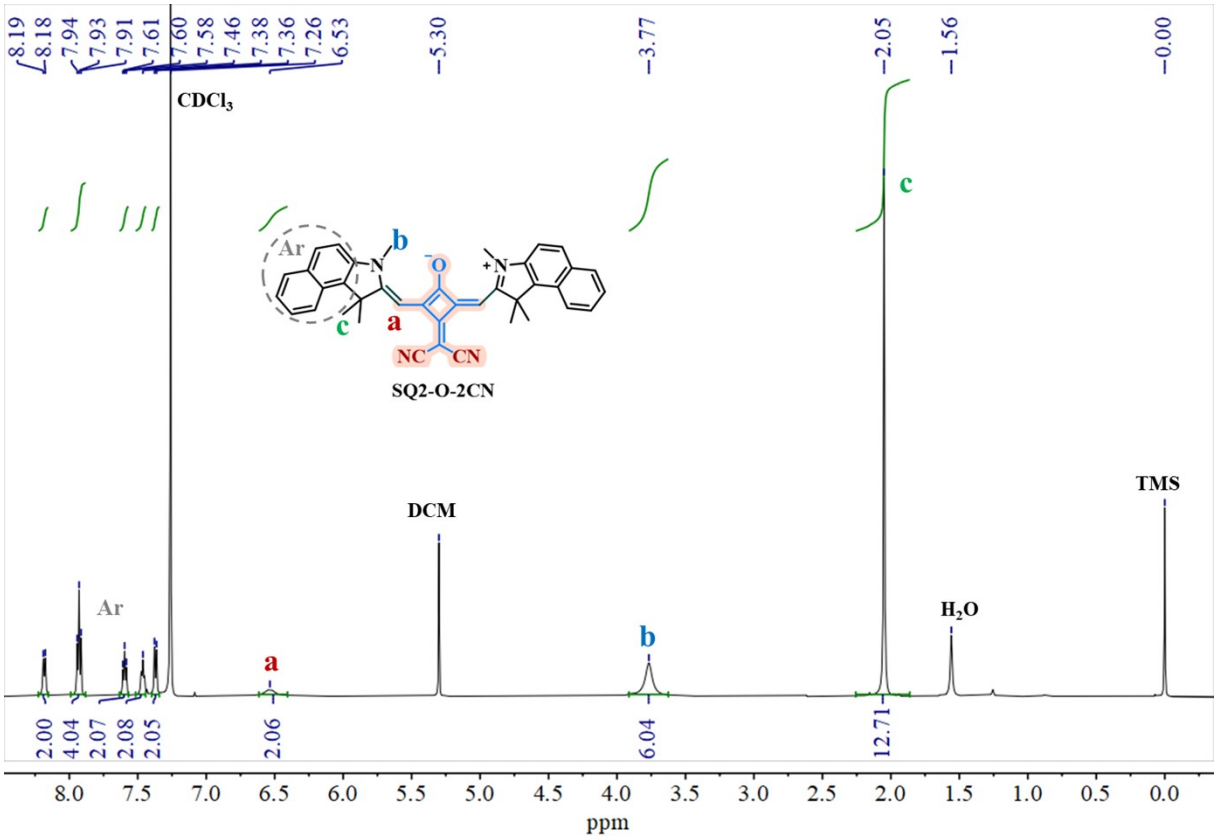

Fig. S38 ^{1}H NMR spectrum of the dye SQ2-O-2CN in $CDCl_3$.

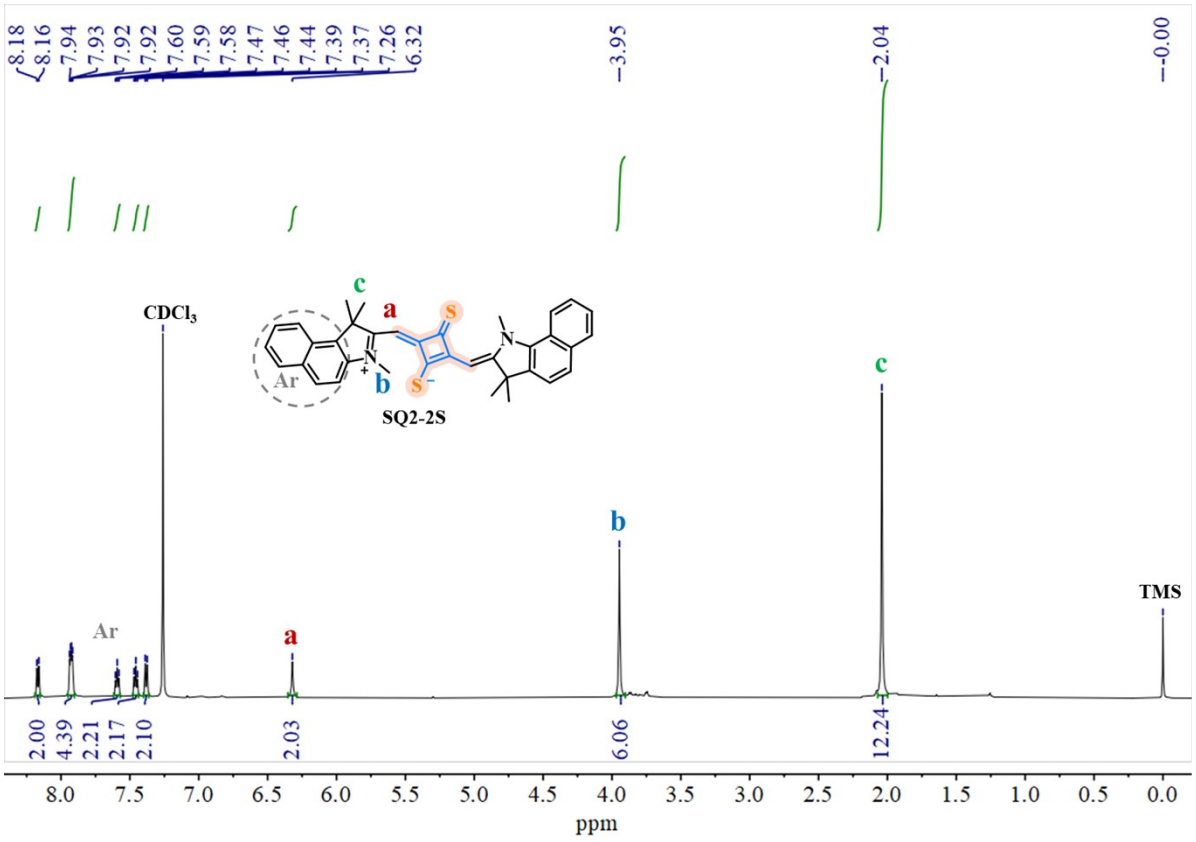

Fig. S39 ^{1}H NMR spectrum of the dye SQ2-2S in $CDCl_3$.

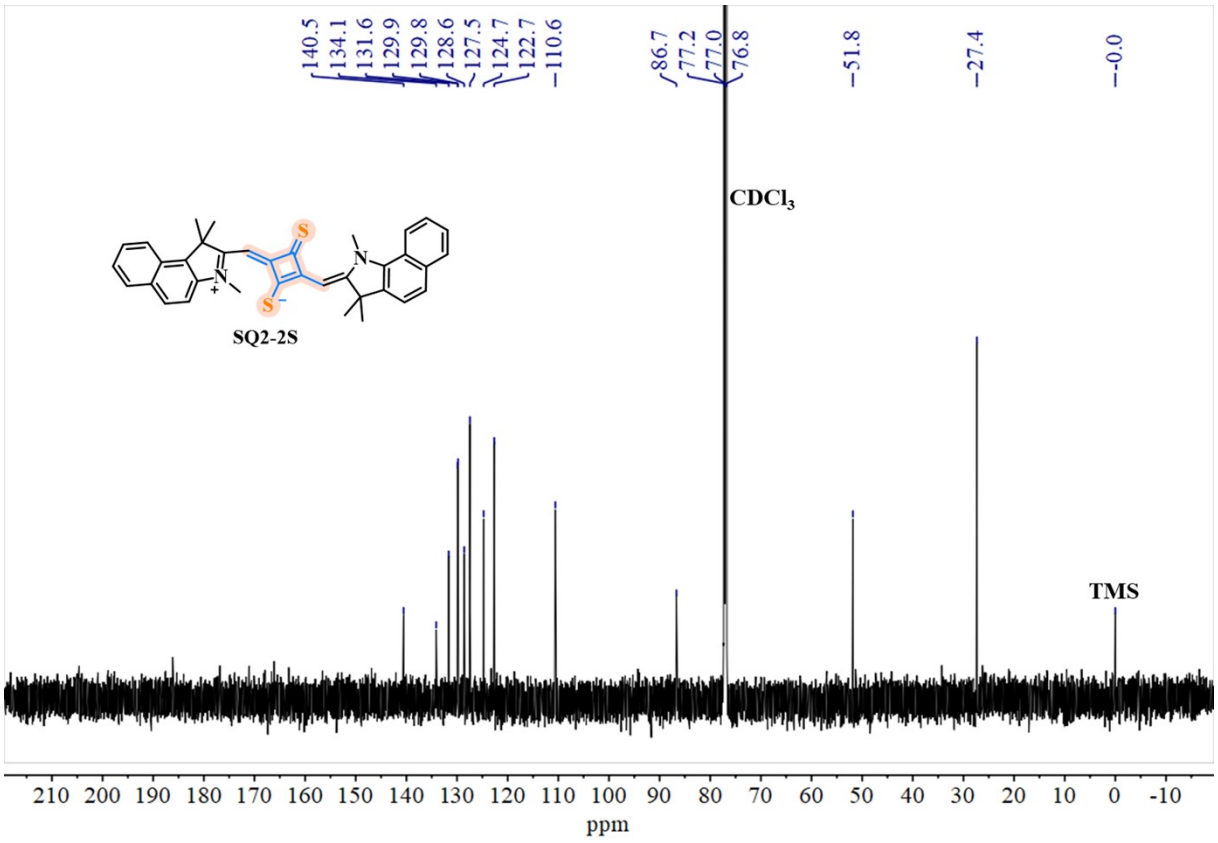

Fig. S40 ^{13}C NMR spectrum of the dye SQ2-2S in $CDCl_3$.

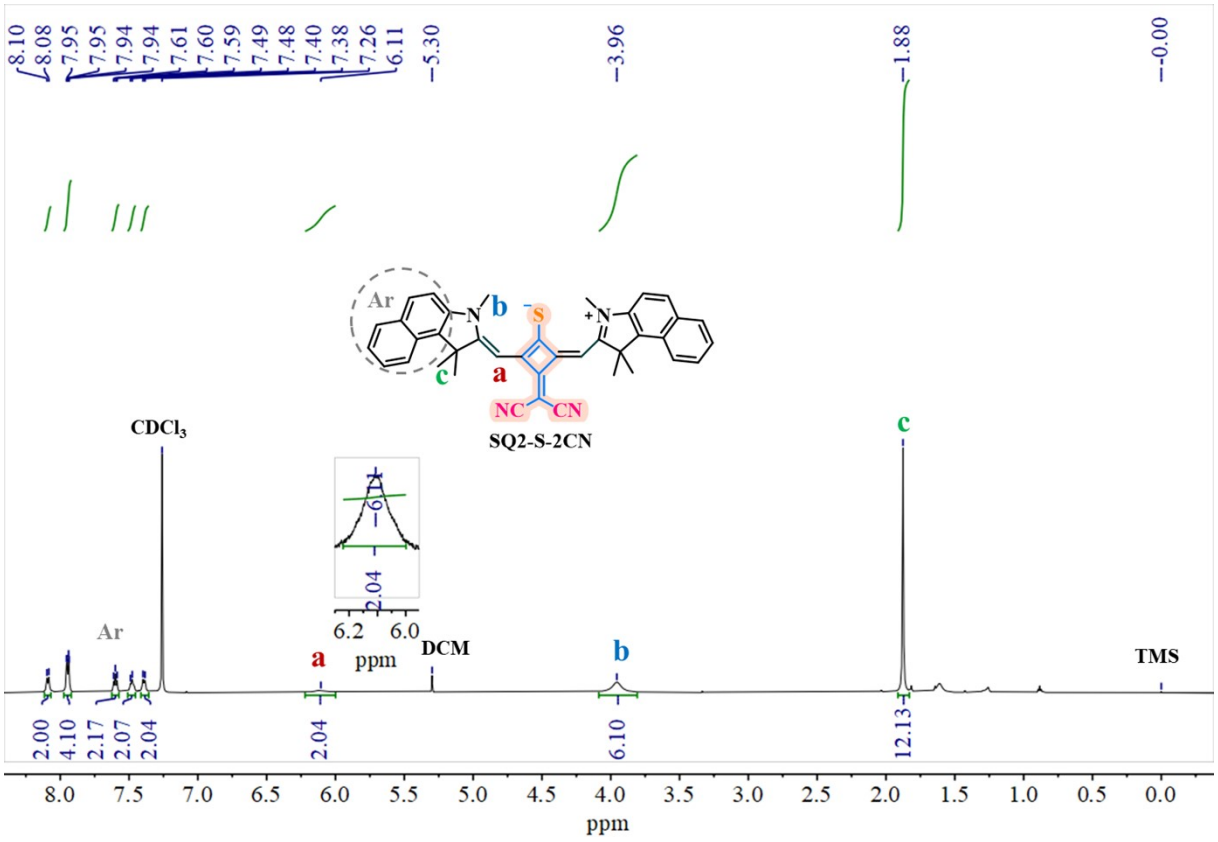

Fig. S41 ^{1}H NMR spectrum of the dye SQ2-S-2CN in $CDCl_3$.

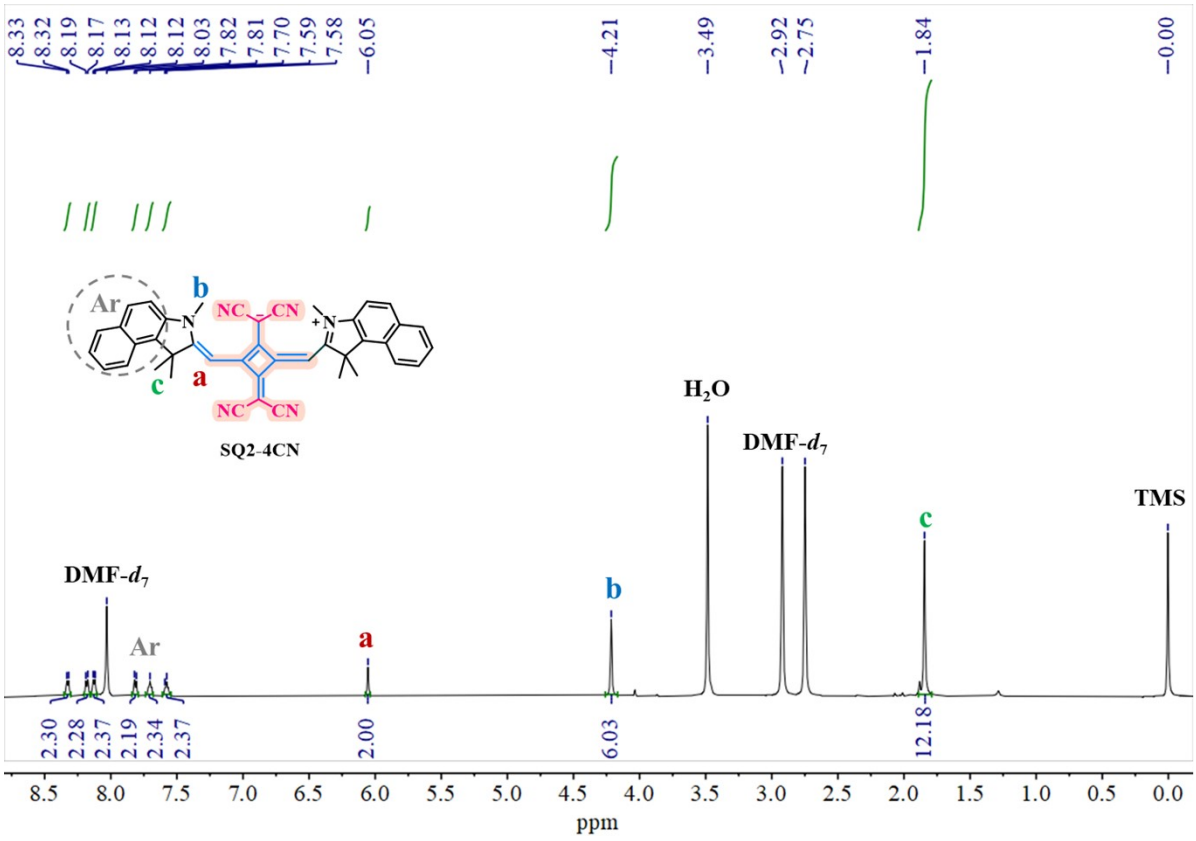

Fig. S42 ^{1}H NMR spectrum of the dye SQ2-4CN in DMF-d_7.

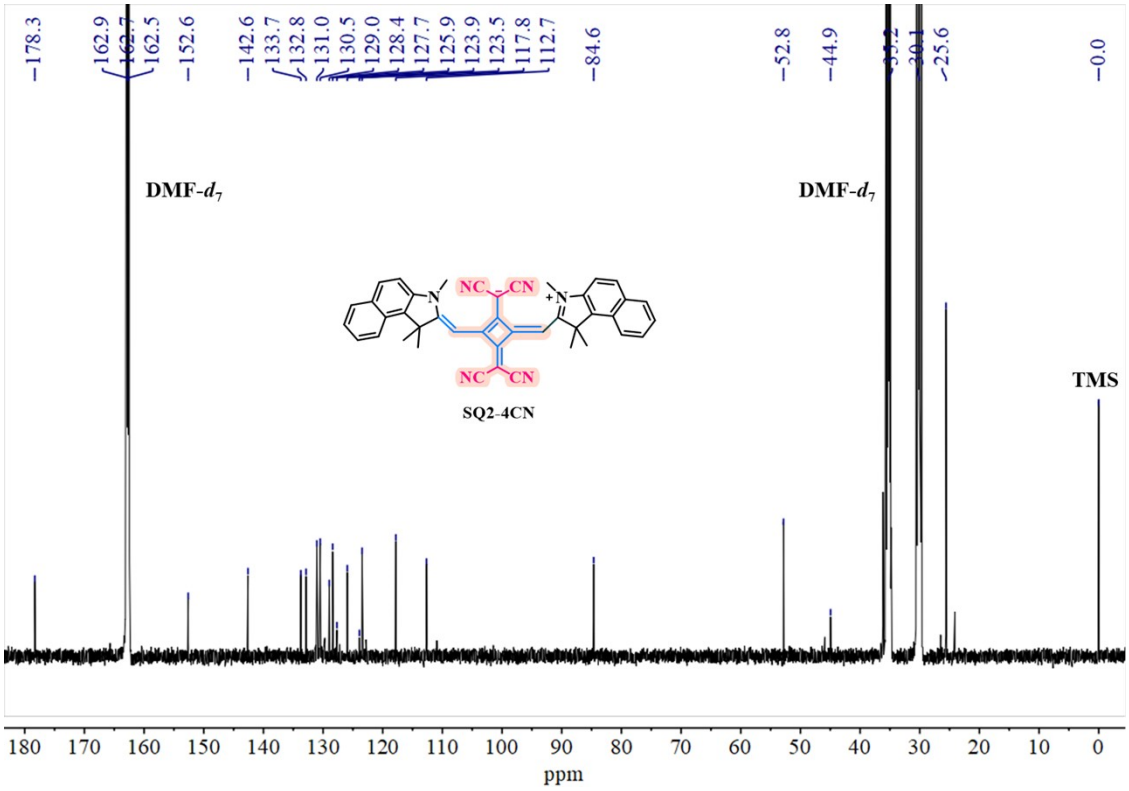

Fig. S43 ^{13}C NMR spectrum of the dye SQ2-4CN in DMF-d_7.

9. HRMS spectra of the dyes

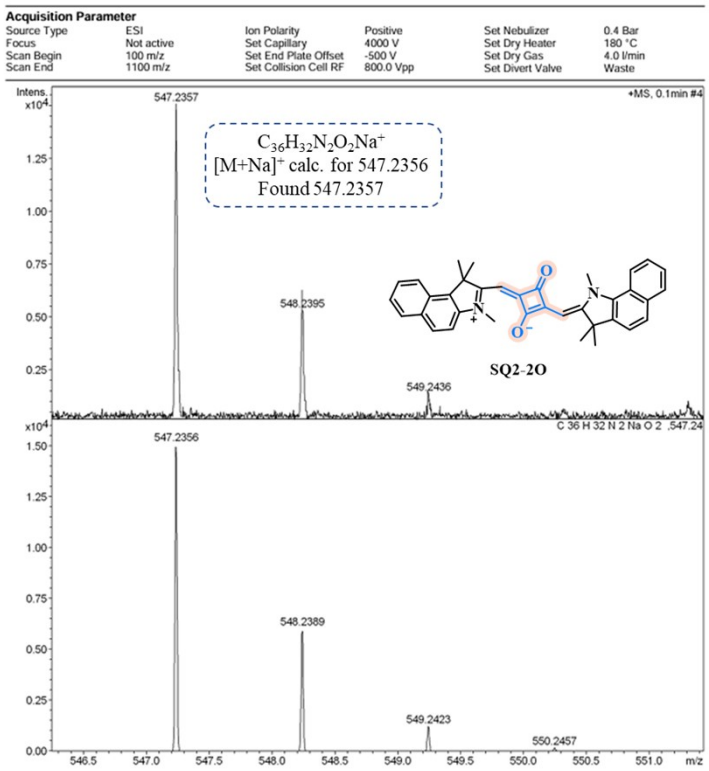

Fig. S44 HRMS spectrum of the dye SQ2-2O.

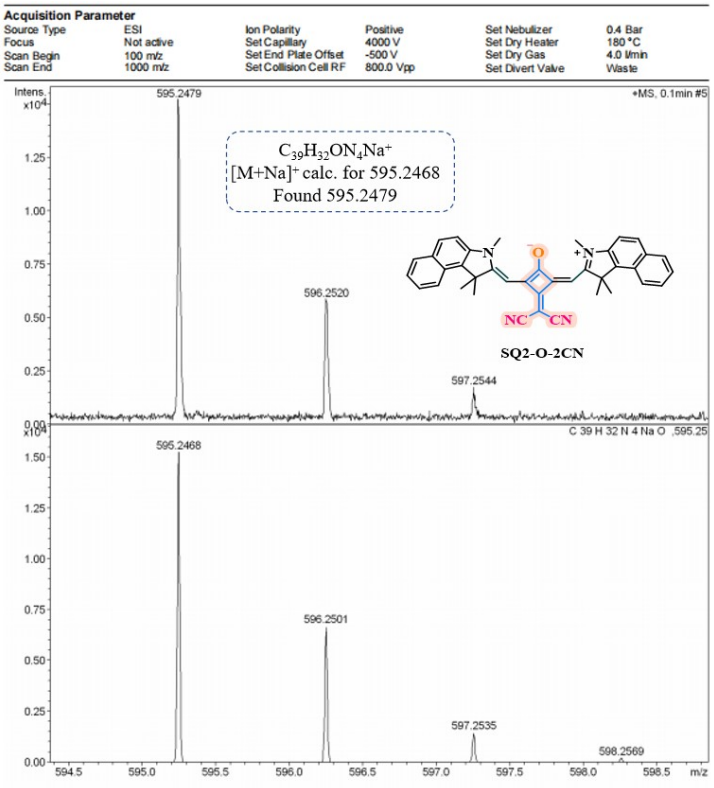

Fig. S45 HRMS spectrum of the dye SQ2-O-2CN.

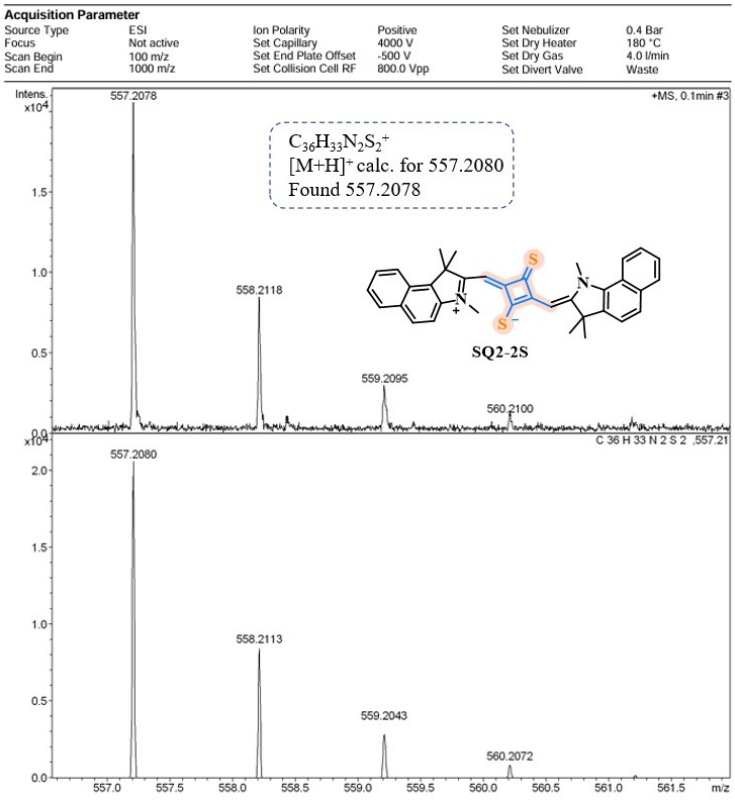

Fig. S46 HRMS spectrum of the dye SQ2-2S.

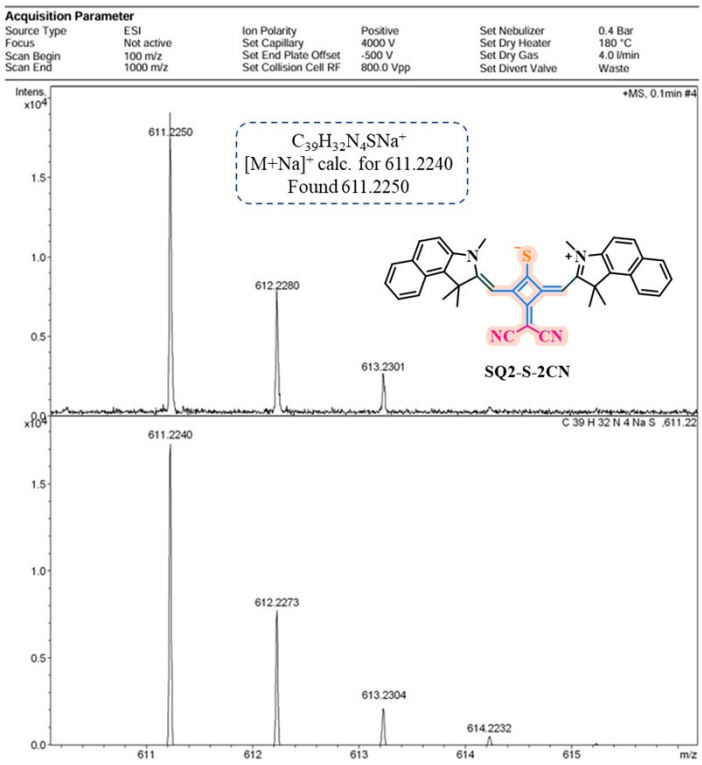

Fig. S47 HRMS spectrum of the dye SQ2-S-2CN.

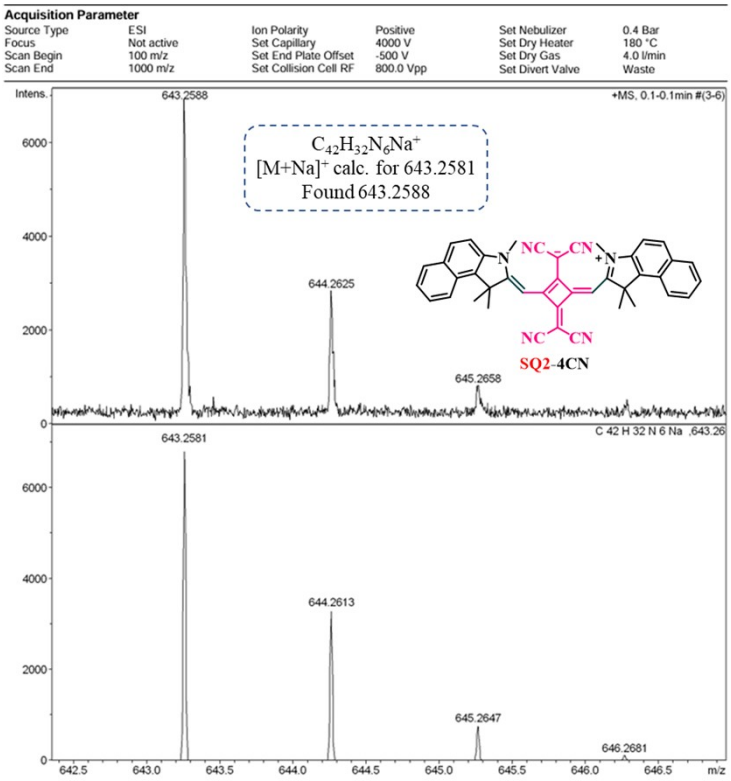

Fig. S48 HRMS spectrum of the dye SQ2-4CN.

References

[1] Zhang N. ; Chang H.; Miao R.; *et al*. Structure-activity relationships of aniline-based squaraines for distinguishable staining and bright two-photon fluorescence bioimaging in plant cells. *J. Mater. Chem. B* **2024**, *12*, 5350-5359.

[2] Li B.; Li Y.; Ping Y.; *et al*. Molecular interface engineering light-driven gellan gum antibacterial films with amplified photothermal-photocatalytic synergy for enhanced cherry tomato preservation. *Chem. Eng. J.* **2026**, *528*, 172489.

[3] Chang H.; Feng J.; Liu X.-A.; *et al*. Ultrafast excited-state dynamics and "three-in-one" phototheranostic properties of a phenanthroline-carbolong photosensitizer. *Chem. Sci.* **2025**, *16*, 7424-7432.

[4] Zhang N.; Liu L.; Chang H.; *et al*. Tunable non-Kasha behaviors and excited-state dynamics of quadrupolar squaraine aggregates. *J. Phys. Chem. Lett.* **2023**, *14*, 7283-7289.

[5] Kurdyukov V. V.; Kurdyukova I. V.; Shishkina S. V.; *et al*. Bis-dicyanomethylene substituted indosquaraine: Synthesis, spectral properties, molecular and crystal structure. *J. Mol. Struct.* **2023**, *1271*, 134038.

[6] Shao M.; Li L.; Yu F.; *et al*. Peroxynitrite activatable double spiral ring derived fluorescent probe for imaging of inflammation and drug-induced liver injury. *Dyes Pigments* **2023**, *215*, 111240.

[7] Mayerhöffer U.; Fimmel B.; Würthner F. Bright near-infrared fluorophores based on squaraines by unexpected halogen effects. *Angew. Chem. Int. Ed.* **2012**, *51*, 164-167.

[8] Kulinich A. V.; Ishchenko A. A. Electronic structure of merocyanine dyes derived from 3H-indole and malononitrile in the ground and excited states: DFT/TD-DFT analysis. *Comput. Theor. Chem.* **2019**, *1154*, 50-56.

[9] Frisch M. J.; Pople J. A.; Binkley J. S. Self-consistent molecular orbital methods 25. Supplementary functions for Gaussian basis sets. *J. Chem. Phys.* **1984**, *80*, 3265-3269.

[10] Maeda T.; Mineta S.; Fujiwara H.; *et al*. Conformational effect of symmetrical squaraine dyes on the performance of dye-sensitized solar cells. *J. Mater. Chem. A* **2013**, *1*, 1303-1309.

[11] Selby J.; Holzapfel M.; Lombe B. K.; *et al*. Chiroptical properties of indolenine squaraines with a stereogenic center at close proximity. *J. Org. Chem.* **2020**, *85*, 12227-12242.

[12] Lu T.; Chen F. Multiwfn: A multifunctional wavefunction analyzer. *J. Comput. Chem.* **2012**, *33*, 580-592.

[13] Feng W.; Jiang Q.; Wang Z.; *et al*. Rigid bay-conjugated perylene bisimide rotors: Solvent-induced excited-state symmetry breaking and resonance-enhanced two-photon absorption. *J. Phys. Chem. B* **2022**, *126*, 4939-4947.

[14] Zang J.; Feng W.; Chang X.; *et al*. Enhanced two-photon absorption of sandwich-like coordination complexes based on squaraine and metallomacrocycle derivatives. *Dyes Pigments* **2021**, *193*, 109487.

[15] Ajami A.; Husinsky W.; Ovsianikov A.; *et al*. Dispersive white light continuum single Z-scan for rapid determination of degenerate two-photon absorption spectra. *Appl. Phys. B* **2018**, *124*, 142.

[16] Liu L.; Li S.; Zhang N.; *et al*. Comparative observation of distinct dynamic stokes shifts in diaryl BODIPY triads with broadband two-photon absorption. *J. Phys. Chem. B* **2023**, *127*, 10171-10178.